Article

TRANSPARENT PROCESS OPEN ACCESS

THE EMBO JOURNAL

Transport through recycling endosomes requires EHD1 recruitment by a phosphatidylserine translocase

Shoken Lee[1,†], Yasunori Uchida[1,†], Jiao Wang[2], Tatsuyuki Matsudaira[1], Takatoshi Nakagawa[3], Takuma Kishimoto[4], Kojiro Mukai[1,4], Takehiko Inaba[4], Toshihide Kobayashi[4], Robert S Molday[2], Tomohiko Taguchi[1,5,*] & Hiroyuki Arai[1,5,**]

Abstract

P_4-ATPases translocate aminophospholipids, such as phosphatidylserine (PS), to the cytosolic leaflet of membranes. PS is highly enriched in recycling endosomes (REs) and is essential for endosomal membrane traffic. Here, we show that PS flipping by an RE-localized P_4-ATPase is required for the recruitment of the membrane fission protein EHD1. Depletion of ATP8A1 impaired the asymmetric transbilayer distribution of PS in REs, dissociated EHD1 from REs, and generated aberrant endosomal tubules that appear resistant to fission. EHD1 did not show membrane localization in cells defective in PS synthesis. ATP8A2, a tissue-specific ATP8A1 paralogue, is associated with a neurodegenerative disease (CAMRQ). ATP8A2, but not the disease-causative ATP8A2 mutant, rescued the endosomal defects in ATP8A1-depleted cells. Primary neurons from *Atp8a2*$^{-/-}$ mice showed a reduced level of transferrin receptors at the cell surface compared to *Atp8a2*$^{+/+}$ mice. These findings demonstrate the role of P_4-ATPase in membrane fission and give insight into the molecular basis of CAMRQ.

Keywords ATP8A1; EHD1; phosphatidylserine; phospholipid flippase; recycling endosomes

Subject Categories Membrane & Intracellular Transport; Neuroscience

DOI 10.15252/embj.201489703 | Received 4 August 2014 | Revised 16 December 2014 | Accepted 17 December 2014 | Published online 16 January 2015

The EMBO Journal (2015) 34: 669–688

Introduction

Membrane-bound organelles of eukaryotic cells have distinct lipid compositions that influence the function of organelles (Behnia & Munro, 2005). Membrane lipids not only serve as a physical barrier, but also interact with a wide variety of integral and peripheral membrane proteins to regulate their localization and activity. Moreover, phospholipids can be distributed asymmetrically between the two leaflets of the lipid bilayer (Devaux, 1992), which provides two distinct surfaces for protein interactions. For example, the cytosolic leaflet of the plasma membrane (PM) is enriched in the aminophospholipids PS and phosphatidylethanolamine (PE), whereas the extracellular leaflet of the PM is enriched in sphingolipids. A low PS concentration in the extracellular leaflet of the PM is crucial for cell life, since phagocytes recognize and engulf cells by the binding to the PS in the surface of target cells (Balasubramanian & Schroit, 2003). A high PS concentration in the cytosolic leaflet of the PM is essential to facilitate various signaling events through membrane translocation and activation of various kinases, such as protein kinase C (Newton & Keranen, 1994) and Akt kinase (Huang *et al*, 2011). In addition to the PM, the membranes of endocytic organelles have asymmetric transbilayer distributions of PS (Fairn *et al*, 2011).

The transbilayer asymmetry of phospholipids is generated, in part, by the selective transport of phospholipids across the membranes (Graham, 2004; Holthuis & Levine, 2005). The P4 subfamily of P-type ATPases (P_4-ATPases) are responsible for the flipping of aminophospholipids to the cytosolic leaflet (Sebastian *et al*, 2012; Coleman *et al*, 2013). The human genome contains 14 P_4-ATPases, and mutations in some P_4-ATPases cause inherited genetic diseases. Mutations in ATP8B1 are associated with familial intrahepatic cholestasis type 1 (Bull *et al*, 1998), and mutations in ATP8A2 are associated with a severe neurological disorder characterized by cerebellar ataxia, mental retardation, and disequilibrium syndrome (CAMRQ) (Onat *et al*, 2013). In mice, mutations in ATP8A2 cause axonal degeneration (Zhu *et al*, 2012) and mutations in ATP11C cause B-cell deficiency syndrome (Siggs *et al*, 2011;

1 Department of Health Chemistry, Graduate School of Pharmaceutical Sciences, University of Tokyo, Tokyo, Japan
2 Departments of Biochemistry and Molecular Biology and Ophthalmology and Visual Sciences, Centre for Macular Research, University of British Columbia, Vancouver, BC, Canada
3 Department of Pharmacology, Osaka Medical College, Takatsuki-city, Osaka, Japan
4 Lipid Biology Laboratory, RIKEN, Wako-shi, Saitama, Japan
5 Pathological Cell Biology Laboratory, Graduate School of Pharmaceutical Sciences, University of Tokyo, Tokyo, Japan
*Corresponding author. Tel: +81 3 5841 4725; Fax: +81 3 3818 3173; E-mail: tom_taguchi@mol.f.u-tokyo.ac.jp
**Corresponding author. Tel: +81 3 5841 4720; Fax: +81 3 3818 3173; E-mail: harai@mol.f.u-tokyo.ac.jp
†These authors contributed equally to this work

Yabas *et al*, 2011). Despite the mounting evidence showing the physiological importance of P_4-ATPases, how their dysfunction causes diseases remains unclear.

REs function in several membrane transport pathways (Mellman, 1996; Maxfield & McGraw, 2004; Taguchi, 2013): the recycling of internalized molecules back to the PM, the exocytic trafficking of several cargoes, and the retrograde transport of internalized molecules to the Golgi. REs also serve as a source of membranes for autophagosomes (Longatti *et al*, 2012; Knaevelsrud *et al*, 2013; Puri *et al*, 2013). We previously showed that evectin-2, an RE protein with a pleckstrin homology (PH) domain, is essential for retrograde traffic (Uchida *et al*, 2011). The PH domain of evectin-2 selectively binds PS *in vitro* and is required for the localization of evectin-2 to REs. The PH domain of evectin-2 faces the cytosol, indicating that PS is present in the cytosolic leaflet of RE membranes. The C2 domain of lactadherin tagged with GFP (GFP-lact-C2) is a widely used PS probe (Yeung *et al*, 2008; Fairn *et al*, 2011). When GFP-lact-C2 was overexpressed in the cytosol, it accumulated at the REs and suppressed the retrograde traffic from REs to the Golgi, indicating that PS at cytosolic leaflet has a critical role in endosomal membrane traffic (Uchida *et al*, 2011). How PS is enriched in the cytosolic leaflet of RE membranes remains unknown.

Eps15 homology domain-containing protein 1 (EHD1) belongs to the EHD-containing or receptor-mediated endocytosis (RME)-1 family, whose members are highly conserved eukaryotic ATPases that have been implicated in membrane remodeling in the endosomal system (Daumke *et al*, 2007; Grant & Caplan, 2008). The human genome contains four EHDs (EHD1-4), one of which (EHD1) is essential for recycling membrane traffic from REs to the PM (Grant *et al*, 2001; Lin *et al*, 2001; Caplan *et al*, 2002). EHD1 is also required for the retrograde membrane transport of Shiga toxin from REs to the Golgi (McKenzie *et al*, 2012). In EHD-1 depleted cells, CD59-positive endosomes became tubulated (Cai *et al*, 2012, 2013). *In vitro*, EHD1 facilitates tubulation or fission of liposomes that contain anionic phospholipids, suggesting that EHD1 functions in the formation of membrane carriers from REs (Pant *et al*, 2009).

Here, we show that a P_4-ATPase (ATP8A1) localizes at REs, regulates the transbilayer asymmetry of PS in the RE membranes, and is essential for the RE localization of EHD1. Together with the observations that EHD1 binds PS *in vitro* and the membrane localization of EHD1 is lost in cells that are defective in PS synthesis, we propose that the PS flipped to the cytosolic leaflet by ATP8A1 is essential for the EHD1 recruitment to REs, thereby regulating the membrane traffic through REs. ATP8A2 is a tissue-specific ATP8A1 paralogue and is associated with a neurodegenerative disease (CAMRQ). ATP8A2, but not the disease-causative ATP8A2 mutant, rescued the endosomal defects in ATP8A1-depleted cells. Primary neurons from *Atp8a2*$^{-/-}$ mice had nearly the same abundance of TfnR as wild-type (WT) neurons, but showed a lower expression of TfnR at the PM. This suggests that ATP8A2 in neurons is essential for recycling membrane traffic and defects in this pathway provide a molecular mechanism for CAMRQ.

Results

ATP8A1 is essential for membrane traffic through REs

Four P_4-ATPases (ATP8A1, ATP9A, ATP11A, and ATP11B) are ubiquitously expressed and localize at early endosomes (EEs) and/or REs (Takatsu *et al*, 2011; Kato *et al*, 2013). Because the ATPase activity of ATP8A1 is strongly activated by PS (Ding *et al*, 2000; Paterson *et al*, 2006; Soupene *et al*, 2008) and because Drs2 (the yeast homologue of ATP8A1) can translocate PS (Zhou & Graham, 2009), we reasoned that ATP8A1 is involved in the enrichment of PS in the cytosolic leaflet of RE membranes.

We first examined the subcellular localization of ATP8A1 in COS-1 cells. COS-1 cells are a cell line with distinctly separate organelles, therefore are suitable for the precise localization of endosomal proteins (Misaki *et al*, 2007) (Supplementary Fig S1). ATP8A1 forms a heteromeric complex with CDC50A, a protein that is essential for the transport of newly synthesized ATP8A1 from the endoplasmic reticulum (ER) (Bryde *et al*, 2010; van der Velden *et al*, 2010). When co-expressed with CDC50A, ATP8A1 co-localized with the RE markers, Rab11 and TfnR, but did not co-localize with other organelle markers [TGN46 (trans-Golgi network), GM130 (cis-Golgi), VPS26 (EEs), CD63 (late endosomes), and LAMP2 (lysosomes)] (Fig 1A). These results showed that ATP8A1 is predominantly localized at REs.

We examined whether ATP8A1 is involved in two membrane transport pathways through REs: the recycling pathway that transports cargoes, such as Tfn/TfnR, from REs to the PM and the retrograde pathway that transports cargoes, such as cholera toxin B subunit (CTxB), from REs to the Golgi. Among three siRNAs designed against human ATP8A1 (siRNA1-3), siRNA1 was the most effective at suppressing ATP8A1 expression (Fig 1B) and was used for the following experiments. For the recycling assay, cells were first pulsed with Alexa 594-Tfn and then chased in media without Alexa 594-Tfn. During the chase, cells were imaged every 6 min for

Figure 1. ATP8A1 regulates endosomal membrane traffic at REs.

A COS-1 cells co-transfected with GFP-ATP8A1 and myc-CDC50A were stained for myc-tag and TfnR, TGN46, GM130, VPS26, CD63, or LAMP2. mCherry-Rab11 was expressed in a cell in the top row. Nuclei were stained with DAPI (in blue). Pearson's coefficient between GFP-ATP8A1 and each organelle marker is shown in the merged image (mean ± SD, $n > 20$ cells from two experiments). Scale bars, 10 μm.

B COS-1 cells were treated with ATP8A1 siRNAs for 72 h. Cell lysates were prepared and then immunoblotted with anti-ATP8A1 antibody. α-tubulin was used as a loading control.

C, D COS-1 cells were treated with ATP8A1 siRNA1 for 72 h. siRNA-resistant GFP-ATP8A1 (WT or E191Q) and myc-CDC50A were transfected 48 h after siRNA transfection. Cells were pulsed with Alexa 594-Tfn and chased in medium with unlabeled Tfn. During the chase, cells were imaged every 6 min for 54 min. The fluorescence intensity of Alexa 594-Tfn is shown as percentage of that at 0 min (mean ± SEM, $n = 4$–6; ***$P < 0.001$; Student's *t*-test). See Supplementary Fig S2 for the representative images.

E, F COS-1 cells were treated with ATP8A1 siRNA1 for 72 h. Cells were pulsed with Alexa 594-CTxB for 5 min and chased for 15 or 60 min. Cells were then fixed and stained for GM130. In (E), representative images are shown. In (F), the Pearson's coefficient between CTxB and GM130 after 60-min chase is shown. Data represent mean ± SD ($n > 26$ cells from three independent experiments). ***$P < 0.001$; two-tailed Student's *t*-test. Scale bars, 10 μm.

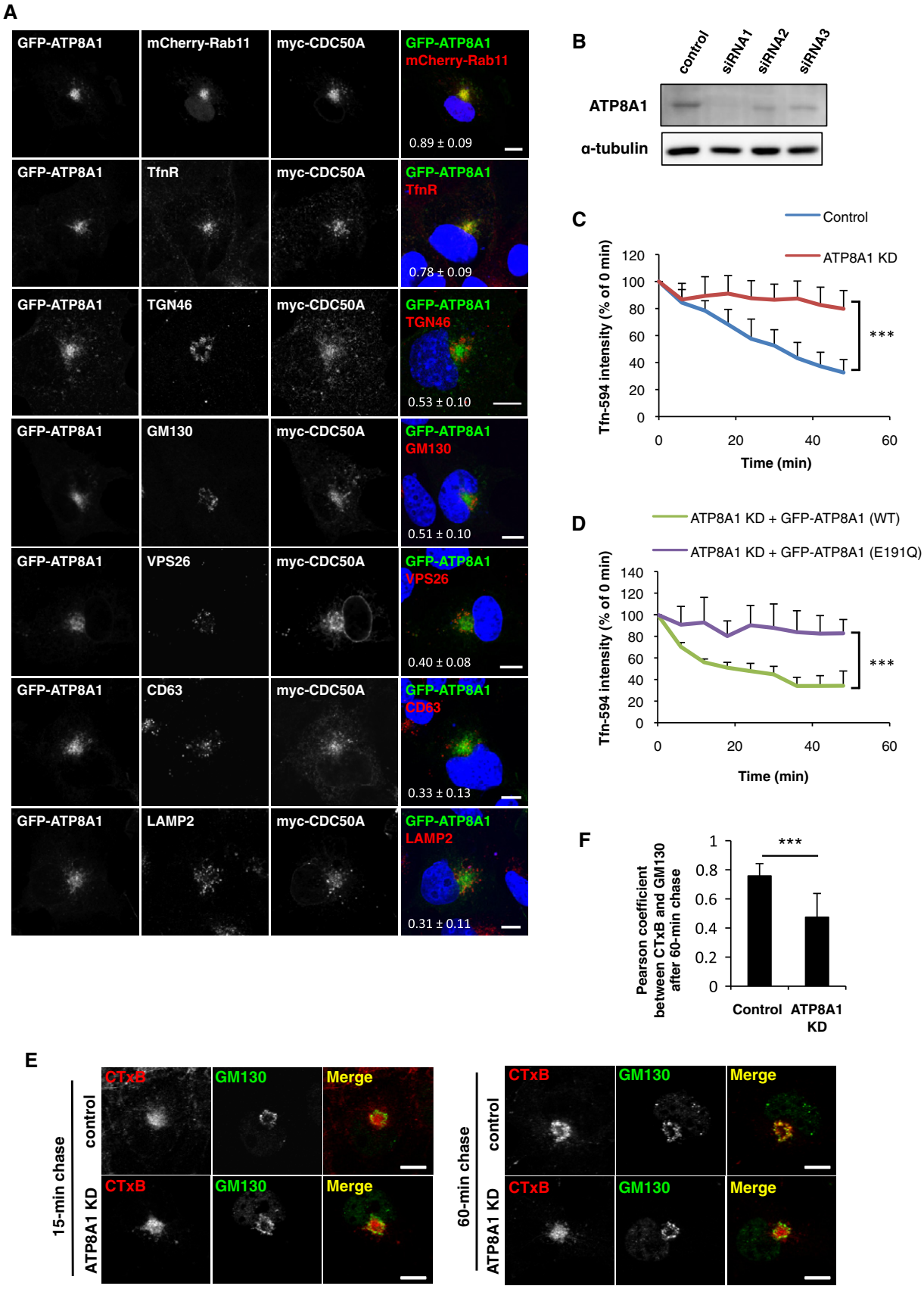

Figure 1.

1 h. After the pulse, Alexa 594-Tfn accumulated at REs in both control and siRNA-treated cells. In control cells, the fluorescence intensity of Alexa 594-Tfn in REs decreased by 50% after a 30-min chase and decreased by 70% after a 50-min chase (Fig 1C and Supplementary Fig S2). In contrast, in ATP8A1-depleted cells, the fluorescence intensity of Alexa 594-Tfn in REs decreased by 10% after a 30-min chase and decreased by 20% after a 50-min chase, suggesting that ATP8A1 is required for efficient recycling of Tfn from REs to the PM. We also performed the rescue experiment by the expression of an siRNA-resistant wild-type ATP8A1. As shown in Fig 1D and Supplementary Fig S2, reinsertion of the wild-type ATP8A1 restored Tfn recycling (not significant versus 'Control' in Fig 1C by Student's *t*-test).

For the retrograde assay, cells were pulsed with Alexa-594 CTxB and then chased for 15 or 60 min. As was shown previously (Uchida *et al*, 2011), CTxB reached REs after a 15-min chase (Fig 1E) and then reached the Golgi after a 60-min chase. In ATP8A1-depleted cells, CTxB reached REs after a 15-min chase as in control cells, but CTxB did not reach the Golgi after a 60-min chase. The colocalization between CTxB and GM130 after a 60-min chase was significantly lower in ATP8A1-depleted cells than in control cells (Fig 1F). Thus, ATP8A1 is required for the retrograde traffic of CTxB from REs to the Golgi.

The endosomal traffic of epidermal growth factor (EGF) from the PM to lysosomes does not pass through REs (Mellman, 1996). After a 5-min pulse/60-min chase of EGF, a portion of EGF co-localized with LAMP1 in control and ATP8A1-depleted cells. Although the LAMP1-positive lysosomes appeared swollen in ATP8A1-depleted cells, no significant difference in the Pearson's coefficient between LAMP1 and EGF was observed (Supplementary Fig S3A and B). This suggests that knockdown of ATP8A1 did not affect the traffic of EGF to LAMP1-positive lysosomes.

Depletion of ATP8A1 induced the formation of aberrant endosomal tubules

Tfn is recycled as a complex with TfnR (Yamashiro *et al*, 1984). The impaired recycling traffic of Tfn in ATP8A1-depleted cells led us to examine the steady-state distribution of TfnR. In control cells, an endogenous TfnR stain showed a bright perinuclear structure and a number of dispersed puncta, which correspond to REs and EEs, respectively (Misaki *et al*, 2007) (Fig 2A). In ATP8A1-depleted cells, although the RE localization of TfnR was basically maintained, TfnR also localized at an extensive array of fine tubules that emanate radially from REs. The tubules were even more obvious in the intensified image. The lengths of some TfnR-positive tubules exceeded 20 μm, nearly reaching the PM (Supplementary Fig S4). The treatment of ATP8A1-depleted cells with nocodazole, a microtubule-depolymerizing agent, disassembled the tubules, indicating that the emergence of TfnR-positive tubules depends on microtubules (Supplementary Fig S4). The staining pattern of VPS26, CD63, or syntaxin 5 (Golgi) was indistinguishable between control and ATP8A1-depleted cells (Fig 2B), suggesting that this tubulation of membranes occurred specifically at REs.

The distribution of TfnR was examined in live cells with the expression of TfnR tagged with GFP. In control cells, TfnR-GFP was mainly found as the mixture of small vesicles and short tubules at REs (Supplementary Fig S5). In contrast, in ATP8A1-depleted cells, TfnR-GFP localized to a number of aberrant tubules, as expected from the observation with endogenous TfnR. Using time-lapse imaging, the dynamics of the TfnR tubules were monitored (Supplementary Movie S1). The tubule marked with a red asterisk retracted over the time monitored and was finally absorbed into REs (Fig 2C). The tubule marked with a green asterisk remained associated with REs. At the time of 0.075 min, small stub with a black asterisk budded from the middle of the tubule but was absorbed by the time of 0.084 min. Few fission events that released TfnR-positive tubules from REs into the cytoplasm were observed.

To determine whether ATP8A1 activity is required for the normal RE distribution of TfnR, we generated an ATPase activity-deficient ATP8A1 mutant. To do this, we mutated Glu191 in human ATP8A1 to Gln because the corresponding Glu198 in bovine ATP8A2, a paralogue of ATP8A1, was found to be essential for its ATPase and flippase activities (Coleman *et al*, 2012). The recombinant Glu191Gln (E191Q) protein complexed with CDC50A was purified to apparent homogeneity (Supplementary Fig S6). The purified WT ATP8A1 showed ATPase activity in a PS-concentration-dependent manner, whereas the E191Q mutant showed only marginal ATPase activity, even when 1 mM PS was included (Fig 2D). We then expressed an siRNA-resistant WT ATP8A1 or E191Q mutant in ATP8A1-depleted COS-1 cells. The number of cells that had TfnR-positive tubules was reduced by the expression of the siRNA-resistant WT ATP8A1 but not by the expression of the siRNA-resistant E191Q mutant (Fig 2E). The expression of E191Q mutant also could not restore Tfn recycling (Fig 1D). Together, these results suggest that normal RE distribution of TfnR and Tfn recycling depend on the ATPase activity of ATP8A1.

The RE localization of EHD1 depends on ATP8A1

The emergence of aberrant TfnR-positive tubules that appear resistant to fission suggests that endosomal membrane fission machinery is dysfunctional in ATP8A1-depleted cells. EHD1 regulates membrane traffic through REs (Grant & Caplan, 2008; McKenzie *et al*, 2012) and facilitates tubulation or fission of liposomes that contain the anionic phospholipids, PS and phosphoinositides (PIPs) (Pant *et al*, 2009). We therefore reasoned that ATP8A1 knockdown would impair EHD1 function.

We first examined the effect of EHD1 knockdown on membrane traffic through REs. siRNA1 designed against EHD1 effectively suppressed EHD1 expression (Fig 3A) and was used for the knockdown experiments. EHD1 knockdown significantly suppressed the recycling of Tfn from REs to the PM (Fig 3B and C) and the retrograde transport of CTxB from REs to the Golgi (Fig 3D; Supplementary Fig S7A). Strikingly, EHD1 knockdown, like ATP8A1 knockdown, resulted in the emergence of aberrant TfnR-positive tubules from REs (Fig 3E; Supplementary Fig S7B). Time-lapse images of EHD1-depleted cells that express TfnR-GFP also showed aberrant TfnR-positive tubules, which appear resistant to fission (Supplementary Fig S7C and Supplementary Movie S2). In summary, EHD1 knockdown phenocopied the ATP8A1 knockdown, in that both impair membrane traffic through REs and generate aberrant TfnR-positive tubules.

We next examined the effect of ATP8A1 knockdown on the subcellular localization of EHD1. Endogenous EHD1 mainly localized perinuclearly and co-localized with GFP-ATP8A1 (Fig 3F), confirming the RE localization of EHD1 as previously described (Lin

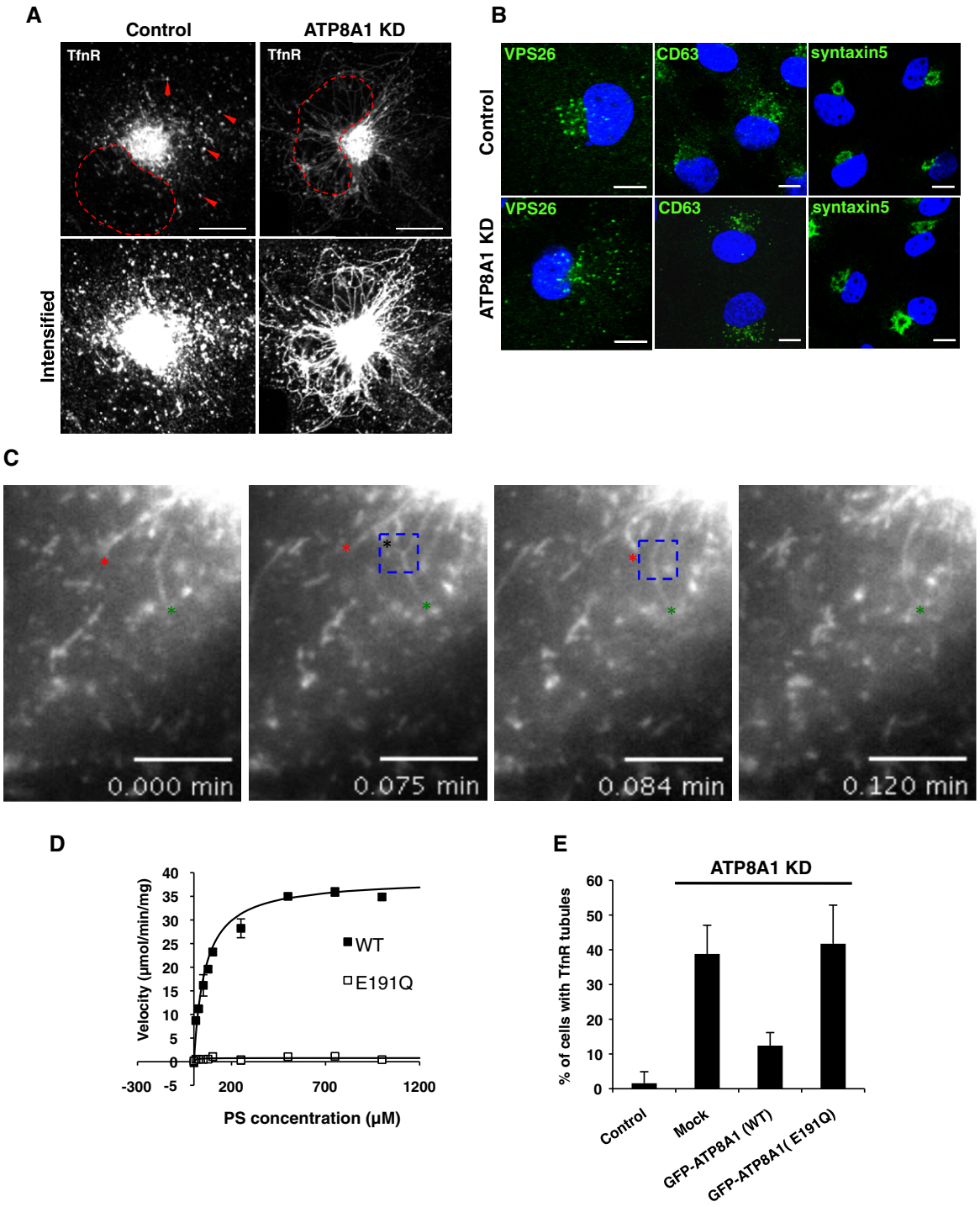

Figure 2. ATP8A1 activity is essential for fission of TfnR-positive membrane carriers.

A COS-1 cells were treated with ATP8A1 siRNA1 for 72 h and stained for TfnR. Each image represents the maximum intensity z-projection of four confocal slices. Intensified images are shown in the bottom row. Red dashed lines and arrowheads indicate nuclei and TfnR puncta, respectively. Scale bars, 10 μm.

B COS-1 cells were treated with ATP8A1 siRNA1 for 72 h and stained for the indicated proteins. Scale bars, 10 μm.

C COS-1 cells were treated with ATP8A1 siRNA1 for 72 h. TfnR-GFP was transfected 48 h after siRNA transfection. Cells were then imaged with an epifluorescent microscope. Selected stills from Supplementary Movie S1 are shown. The asterisks indicate the tips of the tubules of interest. Scale bars, 5 μm.

D The effect of increasing levels of 1,2-dioleoyl-PS on the ATPase activity of purified ATP8A1 (WT and E191Q)-CDC50A complex. The K_m and V_{max} for the WT complex were 59.1 ± 3.5 μM and 38.7 ± 0.8 μmol ATP/min/mg protein, respectively.

E COS-1 cells were treated with ATP8A1 siRNA1 for 72 h. siRNA-resistant ATP8A1 (WT or E191Q), and myc-CDC50A were transfected 48 h after siRNA transfection. Cells were then fixed and stained for TfnR. The graph shows percentages of cells showing aberrant TfnR-positive tubules as mean ± SD of three independent experiments. At least 50 cells were counted per experiment.

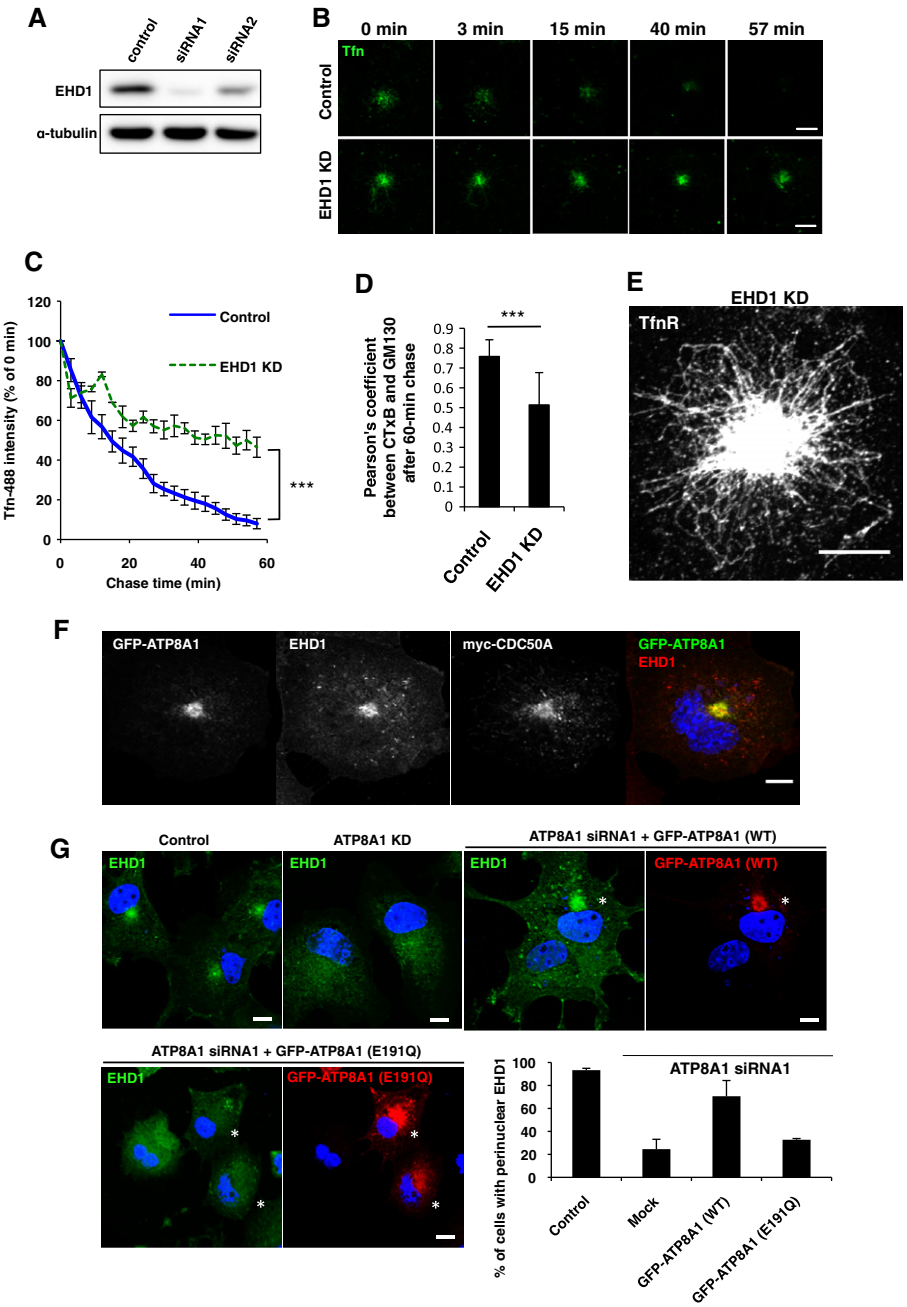

Figure 3. EHD1 localizes at REs in an ATP8A1 activity-dependent manner and is required for fission of TfnR-positive membrane carriers.

A COS-1 cells were treated with EHD1 siRNAs for 72 h. Cell lysates were prepared and then immunoblotted with EHD1 antibody. α-tubulin was used as a loading control.

B, C Cells were treated with EHD1 siRNA1 for 72 h. Cells were pulsed with Alexa 488-Tfn and chased in medium with unlabeled Tfn. During the chase, cells were imaged every 3 min for 57 min. In (B), representative images of Alexa 488-Tfn in control or EHD1-depleted cells are shown. In (C), the fluorescence intensity of Alexa 488-Tfn is shown as percentage of that at 0 min (mean ± SEM, $n > 3$ cells from three independent experiments). ***$P < 0.001$; two-tailed Student's t-test. Scale bars, 10 μm.

D COS-1 cells were treated with EHD1 siRNA1 for 72 h. Cells were pulsed with Alexa 594-CTxB for 5 min and chased for 60 min. Cells were then fixed and stained for GM130. The Pearson's coefficient between CTxB and GM130 is shown (mean ± SD, $n > 30$ cells from two independent experiments). ***$P < 0.001$; two-tailed Student's t-test. See Supplementary Fig S7A for the representative images.

E COS-1 cells were treated with EHD1 siRNA1 for 72 h and stained for TfnR. The image represents the maximum intensity z-projection of four confocal slices. Scale bar, 10 μm.

F COS-1 cells co-transfected with GFP-ATP8A1 and myc-CDC50A were stained for EHD1. Scale bar, 10 μm.

G Cells were treated with ATP8A1 siRNA1 for 72 h and stained for EHD1. For the rescue experiments, siRNA-resistant GFP-ATP8A1 (WT or E191Q) and myc-CDC50A were transfected 48 h after siRNA transfection. Asterisks indicate cells with GFP-ATP8A1 expression. The graph represents percentage of cells with perinuclear localization of EHD1 as mean ± SD of three independent experiments (at least 141 cells were counted for each condition). Scale bars, 10 μm.

et al, 2001). In ATP8A1-depleted cells, EHD1 was not localized at the REs but diffusively distributed in the cytoplasm. The RE localization of EHD1 in ATP8A1-depleted cells was restored by the expression of siRNA-resistant WT ATP8A1, but not by the expression of siRNA-resistant E191Q mutant (Fig 3G). These results suggest that the ATPase activity of ATP8A1 is required for the RE localization of EHD1.

Cellular PS level is critical for EHD1 localization

We reasoned that EHD1 is recruited to REs by phospholipids that are flipped by ATP8A1. The ATPase activity of ATP8A1 is most strongly activated by PS among the various phospholipids (Ding *et al*, 2000; Paterson *et al*, 2006) and ATP8A1 is suggested to flip PS in isolated chromaffin granules (Zachowski *et al*, 1989; Tang *et al*, 1996). However, flipping of PE at the PM is impaired in ATP8A1-depleted cells (Kato *et al*, 2013). The phospholipid specificity of ATP8A1 flippase activity has not been examined in reconstituted systems with purified components.

The ATPase activity of purified recombinant ATP8A1 complexed with CDC50A (Supplementary Fig S6) was assayed in the presence of various lipids. The ATPase activity of ATP8A1 was maximally activated by PS (Fig 4A), in agreement with previous findings (Ding *et al*, 2000; Paterson *et al*, 2006), and to a lesser extent by PE. The flippase activity of ATP8A1 was then measured in liposomes consisting of 97.5% PC and 2.5% NBD-labeled PS or PE. ATP8A1 flipped both NBD-PS and NBD-PE to the same degree (Fig 4B), suggesting that ATP8A1 is not a PS-specific flippase. As expected, the PS flippase activity of the ATP8A1 E191Q mutant that lacks ATPase activity was completely abolished.

Given that ATP8A1 can flip PS and PE, we examined whether the cellular levels of PS and/or PE affect EHD1 localization. In mammals, PS is synthesized by two distinct base-exchange enzymes, PS synthase-I (PSS-I) and PS synthase-II (PSS-II) (Kuge & Nishijima, 1997). PSS-I exchanges serine for the choline of PC, whereas PSS-II exchanges serine for the ethanolamine (Etn) of PE (Fig 4C). A PS-auxotrophic mutant of CHO cells, PSA-3, lacks the activity of PSS-I (Kuge *et al*, 1986). When PSA-3 cells are cultured with dialyzed fetal bovine serum (FBS), which is depleted of Etn, cellular levels of PS and PE decrease by around 30% compared to PSA-3 cells maintained in FBS plus Etn (Lee *et al*, 2012). Under these conditions, the cytoplasmic PS levels drastically decrease, in particular, in REs (Lee *et al*, 2012). EHD1 localization was examined in PSA-3 cells under PS/PE-deficient or PS/PE-rich conditions. Since anti-EHD1 antibody, which was used to stain EHD1 in COS-1 cells, did not stain endogenous EHD1 in CHO cells, GFP-EHD1 was transiently expressed. Unlike in COS-1 cells, GFP-EHD1 expressed in PSA-3 cells under PS/PE-rich conditions localized at discrete tubular compartments as well as perinuclear REs (Fig 4D, arrowhead). In CHO cells, from which PSA-3 cells were derived, EHD1 localized at perinuclear REs and some peripheral tubules (Lin *et al*, 2001). The tubular compartments resemble 'EHD1-positive tubular compartments' that were observed in HeLa cells (Caplan *et al*, 2002). The EHD1-positive tubular compartments are suggested to be a waystation for recycling cargoes from the perinuclear REs to the PM (Grant & Donaldson, 2009; Sharma *et al*, 2009). The different morphologies of EHD1-positive compartments among cell lines may be due to how cells develop post-RE compartments. Despite these differences, under PS/PE-deficient conditions, GFP-EHD1 was evenly distributed into the cytoplasm and not localized to the tubules and perinuclear REs (Fig 4D). These results suggest that the decrease of PS and/or PE levels in cells influences the membrane localization of EHD1.

To dissect the roles of PS and PE in EHD1 localization, another CHO mutant cell line (R-41) was exploited. R-41 cells are defective in the synthesis of PE from PS (Emoto & Umeda, 2000). When R-41 cells are cultured with dialyzed FBS, in a condition where PE synthesis from Etn is suppressed, PE levels decrease by around 40%, whereas PS levels are unchanged (Emoto & Umeda, 2000; Lee *et al*, 2012). Between the two culture conditions: dialyzed FBS plus Etn (PS/PE rich) or dialyzed FBS only (PS rich, PE deficient), the tubular and perinuclear RE localization of EHD1 was indistinguishable (Fig 4E). These results suggest that PE is not an essential determinant for the membrane localization of EHD1. These findings, together with the findings utilizing PSA-3 cells, indicate that PS is critical for the membrane localization of EHD1.

EHD1 binds PS-containing liposomes

To clarify the roles of PS in EHD1 binding, we performed the binding assay with PC-based liposomes that contain different amounts of PS. In brief, His-tagged EHD1 was mixed with liposomes for 15 min, and the mixture was spun at 100,000 *g* for 30 min. The resultant supernatant and pellet were subjected to SDS–PAGE, and the gels were then stained with Coomassie blue for the presence of EHD1 and phospholipids (Boucrot *et al*, 2012). The recombinant EHD1 did not bind to liposomes that do not contain PS (Fig 5A and B). When the PS concentration in liposomes increased, the binding of EHD1 increased sigmoidally (Fig 5C). A sharp increase of the binding of EHD1 was observed from 40 to 70% PS with half-maximal binding at 53% PS. EHD1 did not bind to liposomes that contain 60% PE (Fig 5A and B), but bound to liposomes that contain 60% PI(4,5)P_2 (Supplementary Fig S9A), suggesting that the binding of EHD1 to PS-liposomes is not necessarily through the structure-specific interaction, but rather through the electrostatic interaction.

We next examined the effect of liposome curvature on EHD1 binding. Liposomes with three different diameters were prepared (Supplementary Fig S8). As shown in Fig 5D and E, when the curvature of liposomes increased (*i.e.*, the diameter decreased), more EHD1 bound to liposomes at three PS concentrations examined (20%, 40%, and 60%). These results show that the membrane curvature influences the EHD1 binding to the membranes. The PS concentration required for EHD1 binding to membranes could be lowered by the membrane curvature.

EHD1 is shown to bind to liposomes that contain 10% of PIPs and 10% PS (Blume *et al*, 2007; Pant *et al*, 2009). As Blume *et al* reported, EHD1 bound to liposomes [35% PC, 35% PE, 10% PS, 10% cholesterol, and 10% PI(4)P or PI(4,5)P_2] under our experimental conditions (Supplementary Fig S9B and C). We also examined the binding of EHD1 to liposomes that lack PS [45% PC, 35% PE, 0% PS, 10% cholesterol, and 10% PI(4)P or PI(4,5)P_2] and found that EHD1 did not bind to these membranes (Supplementary Fig S9B and C). These results indicate that PS is required for EHD1 binding to the membranes. Given that EHD1 did not bind to liposomes with a low concentration of PS in the absence of PIPs (Fig 5A and C), other lipid factors may affect the EHD1 binding to the membrane

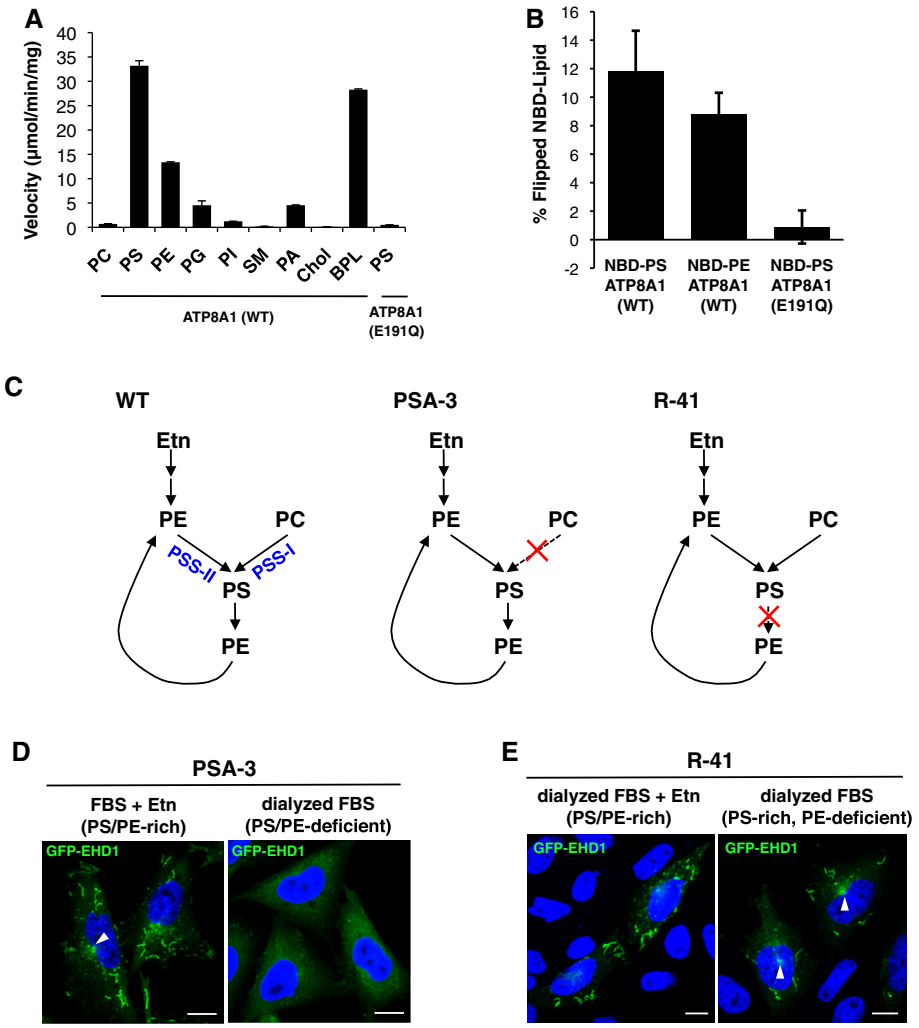

Figure 4. EHD1 localization is dependent on cellular PS levels.

A The effect of various lipids on the ATPase activity of the purified ATP8A1-CDC50A complex. The ATPase activity was measured in the presence of 5 mM ATP and 10 mol % of one of the following lipids: 1,2-dioleoyl-phosphatidycholine (PC), 1,2-dioleoyl-PS, 1,2-dioleoyl-PE, 1,2-dioleoyl-phosphatidylglycerol (PG), 1,2-dioleoyl-phosphatidylinositol (PI), 1,2-dioleoyl-phosphatidic acid (PA), sphingomyelin (SM), cholesterol (Chol), or brain polar lipid (BPL) and 90% PC. The activity of the ATP8A1 (E191Q)-CDC50A in the presence of 1,2-dioleoyl-PS was also determined.

B NBD-labeled PS or PE transport (flippase) activity of ATP8A1 (WT and E191Q)-CDC50A complex. The percentage of NBD-lipid flipped was shown.

C Schematic of the biosynthetic pathway of PS in mammalian cells. The impaired pathways in PSA-3 and R-41 cells are indicated.

D, E PSA-3 and R-41 cells were transiently transfected with GFP-EHD1 and then cultured under the indicated conditions for 72 h. Cells were then fixed, and the nuclei were strained with DAPI. Arrowheads indicate the perinuclear RE localization of GFP-EHD1. Scale bars, 10 μm.

Data information: In (A, B), the data represent the mean ± SD of $n = 3$ independent experiments.

containing PS. As has been reported (Behnia & Munro, 2005; Uchida *et al*, 2011), PIPs were not identified in the RE membrane (Supplementary Fig S10), which suggests that the contribution of PIPs for the EHD1 recruitment to the RE membranes may be minimal.

ATP8A1 knockdown increases PS levels in the luminal leaflet of RE membranes

We hypothesized that ATP8A1 controls the transbilayer distribution of PS in RE membranes. To test this hypothesis, we generated a new PS-specific probe based on the PH domain of evectin-2. The PH domain of evectin-2 specifically binds PS, but with low affinity (Uchida *et al*, 2011). Two evectin-2 PH domains were tandemly connected, hereafter named 2xPH, expressed in *Escherichia coli*, and purified. The recombinant 2xPH retained the PS specificity and had a high affinity for PS (Fig 6A). More than 95% of 2xPH was sedimented with liposomes containing 5% PS, whereas about only 40% of single PH was sedimented with liposomes containing even 20% PS (Uchida *et al*, 2011). Recombinant 2xPH was then applied to cells that had been fixed and treated with 0.1% saponin. Saponin was used to permeabilize RE membranes based on the observations that RE membranes are enriched in cholesterol (Gagescu *et al*, 2000; Mondal *et al*, 2009). Under these conditions, the antibody that recognizes the luminal part of TfnR stained REs, ensuring the

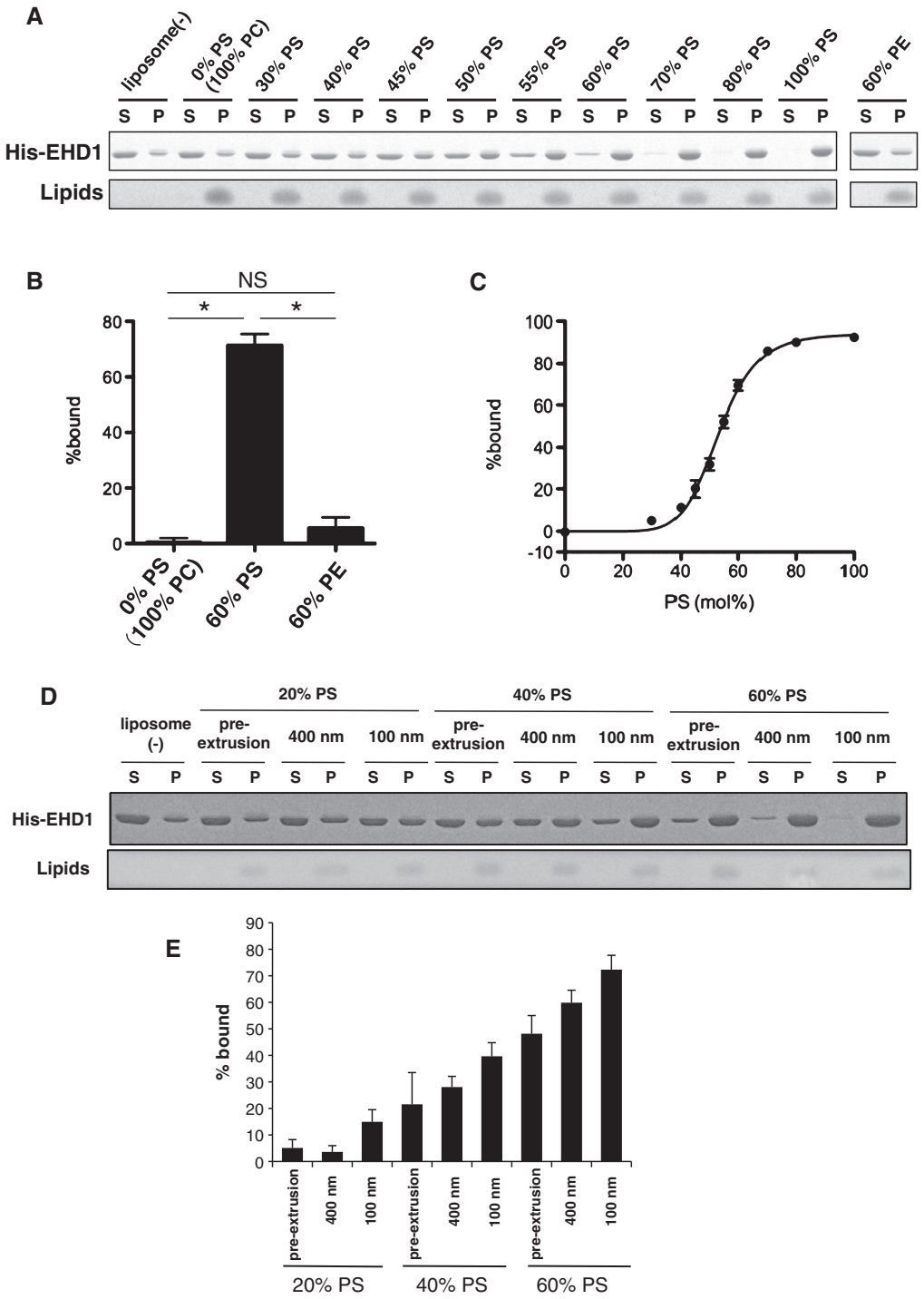

Figure 5. EHD1 binds PS *in vitro*.

A His-tagged EHD1 was mixed with PC-based liposomes containing the indicated % (mol/mol) of PS or PE. After 15 min, the mixture was spun at 100,000 *g* for 30 min, and the resultant supernatant (S) and pellet (P) were subjected to SDS–PAGE. The proteins and lipids were then stained with Coomassie blue.

B, C The intensities of individual bands in (A) were quantified with ImageJ, and the percentage of bound proteins was calculated. In (B), the data represent the mean ± SD of $n = 3$ independent experiments and were analyzed with one-way analysis of variance (ANOVA) followed by Tukey–Kramer *post hoc* test. $^*P < 0.01$; NS, not significant. In (C), each point represents the mean of two independent experiments with an error bar showing the range of values obtained. The sigmoidal fitting was applied.

D, E His-tagged EHD1 was mixed with PC-based liposomes (20, 40, or 60% PS) of decreasing size produced by extrusion through filter pores of the size indicated. After 15 min, the mixture was spun at 100,000 *g* for 30 min, and the resultant supernatant (S) and pellet (P) were subjected to SDS–PAGE. The proteins and lipids were then stained with Coomassie blue. In (E), the intensities of individual bands were quantified (mean ± SEM of three independent experiments). See Supplementary Fig S8 for the size distributions of the prepared liposomes.

permeabilization of RE membranes (Supplementary Fig S11A). 2xPH primarily stained a perinuclear area that co-localized with Tfn (Fig 6B), indicating that RE membranes are enriched in PS compared with other intracellular organelles. It should be noted that the stain of 2xPH under these conditions reflects the presence of PS in both the cytosolic and luminal leaflets of the membranes.

The C2 domain of lactadherin tagged with GFP (GFP-lact-C2) is a widely used PS probe (Yeung *et al*, 2008). GFP-lact-C2 that is expressed in the cytosol binds PS in the cytosolic leaflet, but not in the luminal leaflet of the membranes. As was shown previously (Uchida *et al*, 2011), the cytosolic expression of GFP-lact-C2 strongly stained REs (Fig 6C), indicating that the cytosolic leaflet of the RE membranes is the most enriched with PS.

Using these two PS-specific probes, we examined how PS is distributed between the two leaflets of the RE membranes. Cells were transiently transfected with the GFP-lact-C2 plasmid, then fixed with PFA, permeabilized with saponin, washed, and stained by 2xPH. The image (Fig 6D) showed two representative cells, one that did not express GFP-lact-C2 in the cytosol (indicated by arrowhead) and the other that expressed it (indicated by asterisk). In a cell that did not express GFP-lact-C2, the post-stain by 2xPH clearly visualized REs, as shown above (Fig 6B). In contrast, in a cell that expressed GFP-lact-C2, the post-stain by 2xPH was much fainter than that in a cell that did not express GFP-lact-C2. The intensity of 2xPH at REs in cells with GFP-lact-C2 expression decreased to about 30% of that in cells without GFP-lact-C2 expression (Fig 6E). As mentioned above, GFP-lact-C2, which is expressed in the cytosol, binds PS in the cytosolic leaflet, but not in the luminal leaflet of the membranes. Given that GFP-lact-C2 in the cytosol masks all of the PS in the cytosolic leaflet of the membranes in fixed cells and the fluorescence of the post-stain with 2xPH represents the amount of unmasked PS in the luminal leaflet (Supplementary Fig S11B), this result suggests that 70% of the PS in REs localized in the cytosolic leaflet and the other 30% localized in the luminal leaflet. If any PS in the cytosolic leaflet could not be masked by GFP-lact-C2 and was post-stained by 2xPH, the amount of PS in the cytosolic leaflet should be higher than 70%.

We then examined whether ATP8A1 depletion affects the post-stain by 2xPH at REs. In this experiment, we used COS-1 cells that stably express GFP-lact-C2 in the cytosol. The stain of 2xPH at REs in control cells was as faint as the stain in cells that transiently expressed GFP-lact-C2 (Fig 6D), whereas the stain of 2xPH in ATP8A1-depleted cells was bright with 1.5-fold increase in the fluorescence intensity (Fig 6F and G). The ratio of the fluorescence intensity of 2xPH to that of GFP-lact-C2 was significantly higher in ATP8A1-depleted cells than in control cells (Fig 6H). This result suggests that ATP8A1 flips PS from the luminal to the cytosolic leaflet in RE membranes. On the other hand, EHD1 knockdown did not increase the intensity of post-stain of 2xPH, suggesting that EHD1 did not affect the transbilayer distribution of PS in REs.

ATP8A2 can compensate for the loss of ATP8A1

ATP8A2, a tissue-specific paralogue of ATP8A1, is highly expressed in brain, testis, and retina (Zhu *et al*, 2012). ATP8A2 is the causative gene of wabbler-lethal mice, which show axonal degeneration (Zhu *et al*, 2012). A missense variant of the human ATP8A2 (Ile376Met) has recently been shown to be associated with neurodegenerative disease CAMRQ (Onat *et al*, 2013). Single knockout mice of either ATP8A1 or ATP8A2 are viable, but double knockout mice of ATP8A1 and ATP8A2 are neonatal lethal (Zhu *et al*, 2012), suggesting that the two flippases have redundant roles. We reasoned that ATP8A2, like ATP8A1, is a regulator of endosomal membrane traffic and examined whether ATP8A2 can compensate for the loss of ATP8A1 in COS-1 cells in which no ATP8A2 expression is observed.

GFP-ATP8A2 co-expressed with myc-CDC50A co-localized with TfnR in the perinuclear region (Fig 7A), showing the RE localization of ATP8A2. Like bovine ATP8A2 (Coleman *et al*, 2009), the recombinant human ATP8A2 displayed ATPase activity that was induced by PS (Fig 7B) and PS flippase activity (Fig 7C). In contrast, the disease-associated I376M ATP8A2 mutant displayed little ATPase or flippase activity, consistent with the previous study using the corresponding bovine mutant (I364M) (Vestergaard *et al*, 2014). We then performed a rescue experiment in ATP8A1-depleted cells with the expression of three types of human ATP8A2 (WT, I376M, and E210Q), the latter corresponding to flippase-deficient E198Q of bovine ATP8A2. Although all three ATP8A2 proteins localized primarily at REs, only the WT restored EHD1 localization to REs and resulted in the disappearance of aberrant TfnR-positive tubules (Fig 7D–F). Thus, ATP8A2 can compensate for the loss of ATP8A1 function in a flippase-dependent manner, suggesting that ATP8A2 has a role in the transbilayer distribution of PS in RE membranes.

We then asked whether endogenous ATP8A2 participates in the localization of recycling cargoes such as TfnR. Since ATP8A2 is not ubiquitously expressed (Coleman *et al*, 2009) but expressed in brain (Zhu *et al*, 2012), we used primary cortical neurons that were prepared from *Atp8a2*$^{+/+}$ or *Atp8a2*$^{-/-}$ mice (Coleman *et al*, 2014). Although the total amounts of TfnR in *Atp8a2*$^{-/-}$ and *Atp8a2*$^{+/+}$ neurons were comparable, the ratio of surface TfnR to total TfnR was dramatically reduced in *Atp8a2*$^{-/-}$ neurons (Fig 7G and H). These results imply that ATP8A2 functions in recycling membrane traffic to the PM in neurons.

Discussion

In the present study, we showed in mammalian cells that a P_4-ATPase ATP8A1 translocates PS from the luminal leaflet to the cytosolic leaflet in the RE membranes. We also found that a membrane fission protein EHD1, which binds PS *in vitro*, is dispersed from REs to the cytoplasm by ATP8A1 depletion. Cells depleted of ATP8A1 generate extensively tubulated membranes from REs, which appear resistant to fission. Cells depleted of EHD1 also generate tubular membranes from REs. From these results, we propose that the flipping of PS to the cytosolic leaflet by a P_4-ATPase is critical for recruiting a membrane fission protein to the RE membranes and generating transport vesicles from REs. Studies in *Saccharomyces cerevisiae* have shown that a P_4-ATPase Drs2, which flips PS and to a lesser extent PE, is essential for membrane traffic between the late Golgi compartment and endosomes (Sebastian *et al*, 2012) and that other P_4-ATPases Dnf1 and Dnf2, which flip phospholipids such as PC and PE, participate in endocytic vesicle formation (Pomorski *et al*, 2003). In *Caenorhabditis elegans*, a P_4-ATPase TAT-1 is most closely related to mammalian ATP8A1. The loss of *tat-1* leads to the generation of abnormal endo-lysosomal compartments, suggesting that endocytic cargo sorting and recycling are impaired (Ruaud *et al*, 2009; Chen *et al*, 2010). In *Arabidopsis thaliana*, a P_4-ATPase ALA3 that localizes

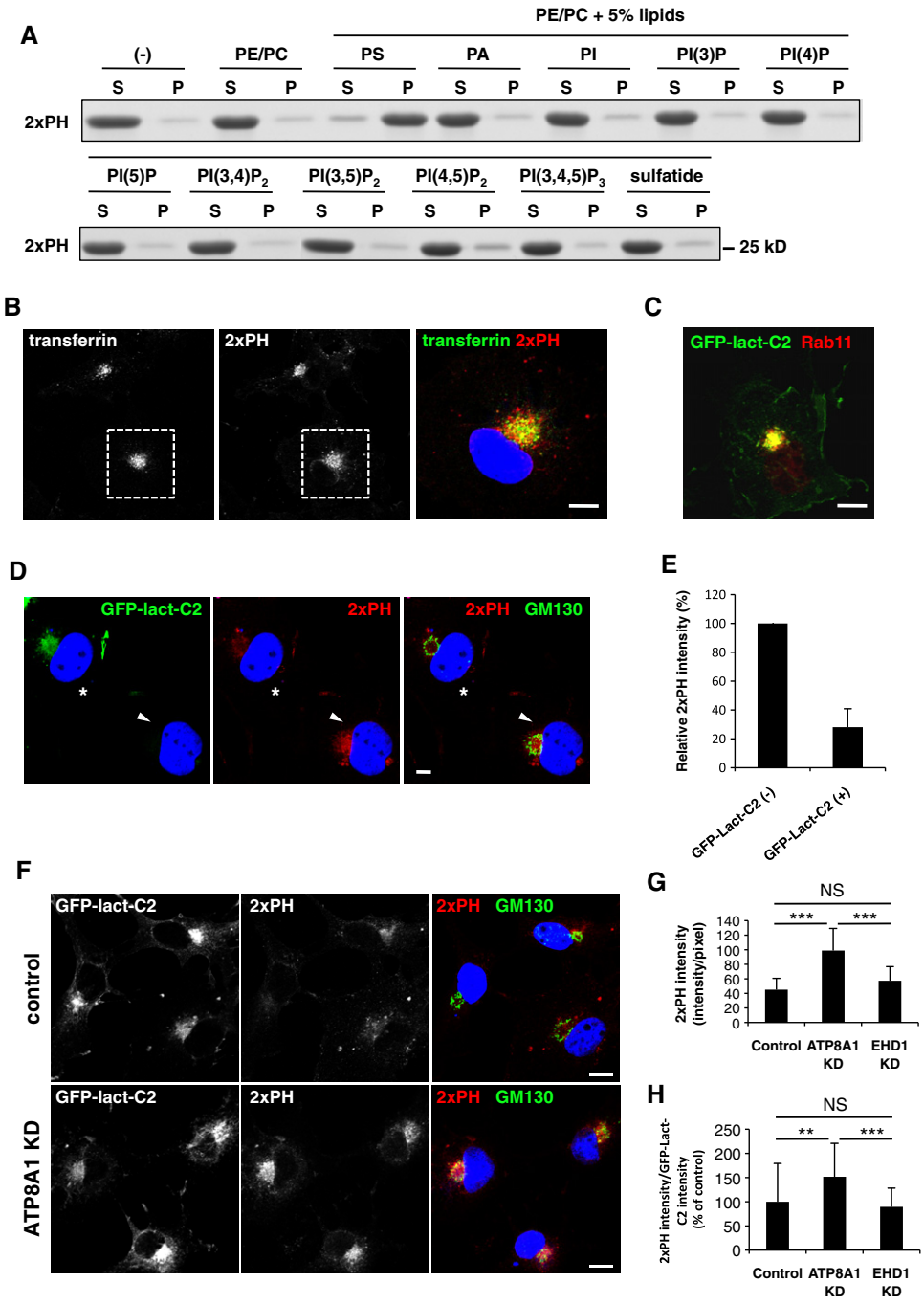

Figure 6. ATP8A1 knockdown causes an increase in RE luminal PS levels.

A His-tagged 2xPH was mixed with liposomes that were composed of 75% (mol/mol) PE, 20% (mol/mol) PC, and 5% (mol/mol) of PS, PA, PI, PIPs, or sulfatide. In the case of PE/PC, liposomes of 80% (mol/mol) PE and 20% (mol/mol) PC were used. After 15 min, the mixture was spun at 100,000 *g* for 30 min, and the resultant supernatant (S) and pellet (P) were subjected to SDS–PAGE. The gels were stained with Coomassie blue.

B COS-1 cells were incubated in medium containing Alexa 488-Tfn for 40 min, washed, fixed, and stained with recombinant 2xPH. Magnified image is shown in the right panel. Scale bar, 10 μm.

C COS-1 cells were transiently transfected with GFP-lact-C2 and stained for Rab11. Scale bar, 10 μm.

D, E COS-1 cells were transiently transfected with GFP-lact-C2 and stained with recombinant 2xPH and anti-GM130 antibody. The asterisk indicates a cell expressing GFP-lact-C2, and the arrowhead indicates a non-expressing cell. The graph in (E) shows fluorescence intensity per pixel of recombinant 2xPH stain in RE area, which was delimited by GM130. Data are normalized to the 2xPH intensity in GFP-lact-C2 (–) cells (mean ± SD, n = 13 cells for each condition). Scale bar, 10 μm.

F–H COS-1 cells stably expressing GFP-lact-C2 were treated with ATP8A1 siRNA1 or EHD1 siRNA1 for 72 h and stained with recombinant 2xPH and anti-GM130 antibody. The intensities of 2xPH staining and GFP-lact-C2 in RE area were measured. The intensity of 2xPH (G) and the ratio of 2xPH to GFP-lact-C2 intensities (H) are shown. In (H), data are normalized to that of control cells. Data represent mean ± SD and were analyzed with two-tailed Student's t-test (n > 26 cells from three independent experiments). **P < 0.01; ***P < 0.001; NS, not significant. Scale bars, 10 μm.

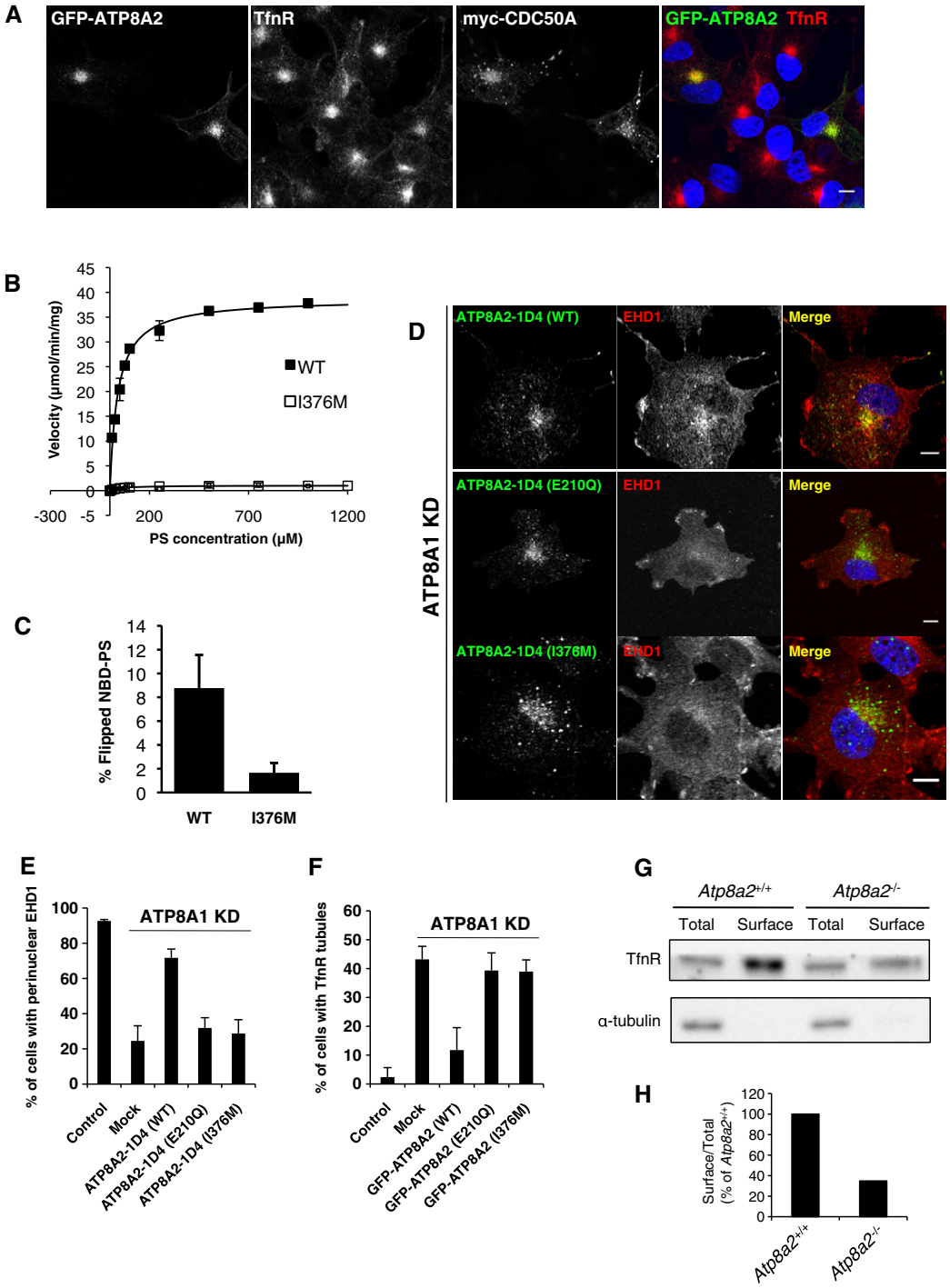

Figure 7. Wild-type ATP8A2, but not a disease-associated mutant, can compensate for the loss of ATP8A1 function.

A COS-1 cells co-transfected with GFP-ATP8A2 (WT) and myc-CDC50A were stained for myc-tag and TfnR. Scale bar, 10 μm.

B The effect of increasing levels of PS on the ATPase activity of ATP8A2 (WT and I376M)-CDC50A complex.

C NBD-labeled PS transport (flippase) activity of ATP8A2 (WT and I376M)-CDC50A complex. The percentage of NBD-lipid flipped was shown.

D Cells were treated with ATP8A1 siRNA1 for 72 h. ATP8A2-1D4 (WT or mutants) and myc-CDC50A were transfected 48 h after siRNA transfection. The cells were then stained for EHD1 and 1D4-tag. Scale bars, 10 μm.

E Quantification of percentages of cells with perinuclear EHD1 localization. Data represent mean ± SD of three or four independent experiments. At least 20 cells were counted per experiment.

F Cells were treated with ATP8A1 siRNA for 72 h. GFP-ATP8A2 (WT or mutant) and myc-CDC50A were transfected 48 h after siRNA transfection. The cells were then stained for TfnR. Data represent mean ± SD of three or four independent experiments. At least 20 cells were counted per experiment.

G, H Surface biotinylation assay with *Atp8a2*$^{+/+}$ or *Atp8a2*$^{-/-}$ cortical neurons. The ratio of surface to total TfnR was quantified and normalized to *Atp8a2*$^{+/+}$. Data represent mean value (2 mice for each genotype).

at the Golgi is essential for the formation of secretory vesicles (Poulsen *et al*, 2008). Thus, these studies, together with the present finding in mammalian cells, indicate that the function of phospholipid flippases in vesicular membrane traffic is evolutionally conserved from lower eukaryotes to mammals. In the *C. elegans tat-1* mutant, an EHD1 homologue, RME-1, still localized at abnormal endo-lysosomes (Chen *et al*, 2010). We cannot explain at the present time the apparent discrepancy on the localization of EHD1/RME-1 in the loss of ATP8A1/TAT-1.

One hypothesis for the mechanism by which P_4-ATPases function in the vesicular membrane traffic is that P_4-ATPases generate membrane curvature through unidirectional movement of phospholipids, which facilitates membrane budding to form transport vesicles together with budding machinery (Sebastian *et al*, 2012). Recently, *S. cerevisiae* Gcs1, which is an Arf GTPase-activating protein and regulates retrograde transport from endosomes to the late Golgi, was shown to have an +ALPS-motif that binds highly curved membranes with anionic phospholipids including PS (Xu *et al*, 2013). Importantly, the localization of Gcs1 to the late Golgi/endosomes is regulated by Drs2. Our study in mammalian cells provides another mechanistic insight into the site of action of P_4-ATPases: PS flipped by ATP8A1 to the cytosolic leaflet recruits a membrane fission protein EHD1 that has an ability to bind PS, thereby regulating the membrane fission process.

PS comprises 5–10% of the total phospholipids in mammalian cells (Vance & Steenbergen, 2005; Lee *et al*, 2012). PS is fivefold more abundant in the purified RE fraction than in the cell lysate (Gagescu *et al*, 2000), suggesting that PS accounts for 25–50% of the total phospholipids in RE membranes. Using two PS-specific probes, we roughly estimated that 70 and 30% of PS are localized in the cytosolic and the luminal leaflets of RE membranes, respectively. Taking this PS asymmetry into consideration, PS may comprise 35% ($= 25 \times 2 \times 0.7$) − 70% ($= 50 \times 2 \times 0.7$) of total phospholipids in the cytosolic leaflet of RE membranes. PS is also enriched and asymmetrically distributed in the cytosolic leaflet of the PM (Devaux, 1992). A study using red blood cells, which lack intracellular organelles, showed that PS comprises 15% of total phospholipids (Dodge & Phillips, 1967), suggesting that PS comprises about 30% of the total phospholipids in the cytosolic leaflet of the PM. Therefore, the abundance of PS in the cytosolic leaflet of RE membranes could be comparable or even higher than that in the PM. This high concentration of PS in the cytosolic leaflet of RE membranes, which is produced by a P_4-ATPase ATP8A1, might be enough to recruit EHD1 specifically to REs, since the half-maximal binding of EHD1 to PS was observed at ~50% PS in the liposome co-sedimentation assay.

Despite the increase of PS in the luminal leaflet in ATP8A1-depleted cells, PS was still present in the cytosolic leaflet of RE membranes as the PS probe expressed in the cytosol significantly stained REs in ATP8A1-depleted cells. The presence of PS in the cytosolic leaflet of RE membranes was also supported by the observation that evectin-2, a protein that requires PS in the cytosolic leaflet for its RE localization (Uchida *et al*, 2011), localized at REs in ATP8A1-depleted cells (Supplementary Fig S12). Thus, although ATP8A1 contributes to the enrichment of PS in the cytosolic leaflet of RE membranes, its knockdown does not result in the complete disappearance of PS at the cytosolic leaflet. Scramblases that mediate bidirectional transbilayer movement of phospholipids or other P_4-ATPases may participate in the exposure of PS at the cytosolic leaflet in ATP8A1-depleted cells. PS is synthesized in the cytosolic leaflet of the ER and likely moves via non-vesicular routes (Maeda *et al*, 2013) and/or vesicular routes to the PM and other organelles. These processes (Holthuis & Menon, 2014) may also contribute to the localization of PS in the cytosolic leaflet of the RE membranes.

EHD proteins contain an amino-terminal ATP-binding G-domain, followed by a helical domain and a carboxy-terminal EH domain (Grant & Caplan, 2008). The crystal structure of full-length EHD2 was solved (Daumke *et al*, 2007). Dimerization of G-domain creates a putative membrane-binding surface with a polybasic stretch within the helical domain (residues 285–400). EHD2 mutants (F322A, K324D, K327D, K328D, or K329D) display a completely cytoplasmic distribution, showing the critical role of these amino acids in the helical domain in membrane localization of EHD2 (Daumke *et al*, 2007). EHD1 (K324D) lost its membrane localization in COS-1 cells similar to EHD2 (K324D) and did not bind to PS-liposomes *in vitro* (Supplementary Fig S13), which supports the idea that PS is essential for binding of EHD1 to the membranes. We noticed that when expressed in COS-1 cells, GFP-EHD1 localized at perinuclear REs and cytoplasmic tubular structures (Supplementary Fig S13). The latter was not obvious when endogenous EHD1 was immuno-stained (Fig 3). The tubular structures may correspond to 'tubular recycling compartments' in HeLa cells (Caplan *et al*, 2002). EHD1 that lacks EH-domain (ΔEH) still localized at perinuclear REs, but not at cytoplasmic tubular structures (Supplementary Fig S13). This observation is consistent with the previous report that ΔEH did not localize at tubular recycling compartment in HeLa cells (Caplan *et al*, 2002). However, ΔEH mutant bound to PS-liposomes *in vitro* (Supplementary Fig S13). These results suggest that PS is not the sole determinant for EHD1 localization at cytoplasmic tubular structures. Recruitment of EHD1 to tubular structures in HeLa cells requires the interactions between EH domain and NPF-containing proteins, such as MICAL-L1 (Sharma *et al*, 2009) and Pacsin (Giridharan *et al*, 2013). It is also proposed that MICAL-L1 and Pacsin bind to phosphatidic acid in the tubular structures (Giridharan *et al*, 2013). It is tempting to speculate that there are two distinct recycling compartments, perinuclear REs to which EHD1 is recruited primarily by PS and tubular recycling compartment to which EHD1 is recruited cooperatively by phosphatidic acid and PS.

Recent studies have revealed the significance of PS in the cytosolic leaflet of endosomes (reviewed in Bigay & Antonny, 2012; Holthuis & Menon, 2014). As mentioned above, *S. cerevisiae* Gcs1 has a+ALPS-motif that binds highly curved membranes with anionic phospholipids that include PS (Xu *et al*, 2013). Gcs1 localizes at the late Golgi/endosomes and its localization is regulated by a P_4-ATPase Drs2, suggesting that PS flipped by Drs2 is essential for Gcs1 recruitment. K-Ras is a major proto-oncogene product (Hancock, 2003). K-Ras mainly localizes at the PM, but some of it localizes at endosomes (Lu *et al*, 2009; Gelabert-Baldrich *et al*, 2014). K-Ras has a polybasic stretch at the carboxy-terminus that electrostatically interacts with PS (Yeung *et al*, 2008). This interaction was recently shown to be essential for K-Ras trapping at REs, from where vesicular transport delivers K-Ras to the PM (Schmick *et al*, 2014). Evectin-2 that localizes at REs has a PH domain that binds PS but not PIPs. This PH domain is essential for the RE localization of evectin-2 and the regulation of the retrograde traffic from REs to the Golgi (Uchida *et al*, 2011). These findings, together with the present study, indicate that PS in REs has multifaceted functions

in membrane traffic, such as cargo collection, membrane budding, and membrane fission. Other membrane systems, including PM, EEs, LEs, and the Golgi, exploit PIPs to exert their own functions through a variety of PIP effectors (Behnia & Munro, 2005; Di Paolo & De Camilli, 2006). Importantly, the levels of PIPs are tightly regulated by phosphorylation and dephosphorylation. As far as we know, the metabolic conversion of PS is confined to the ER and/or mitochondria in mammalian cells (Vance & Steenbergen, 2005). Therefore, in other cellular membranes, cells may exploit the lipid flipping system by P_4-ATPases to regulate the local levels of cytosolic PS. It is also noted that Drs2p in the trans-Golgi network is activated by PI(4)P (Natarajan *et al*, 2009), suggesting that PIPs could control the PS content in the cytosolic leaflet of the membranes.

ATP8A2 is a paralogue of ATP8A1, and mutations of ATP8A2 cause axonal degeneration in mice (wabbler-lethal mice) (Zhu *et al*, 2012) and are associated with neurodegenerative disease CAMRQ in humans (Cacciagli *et al*, 2010; Onat *et al*, 2013). However, cellular mechanism of ATP8A2 has been unclear. The present study showed that ATP8A2 localized at REs and could compensate for the loss of ATP8A1 when expressed in COS-1 cells. In contrast, the disease-causative human ATP8A2 mutant (I376M), which lacked ATPase and flippase activities, could not rescue the loss of ATP8A1. Furthermore, primary cortical neurons isolated from *Atp8a2*$^{-/-}$ mice showed a drastic reduction of TfnR present in the PM, with the total amount of TfnR being comparable to that in primary cortical neurons isolated from *Atp8a2*$^{+/+}$ mice. These findings suggest that ATP8A2 functions in endosomal membrane traffic through REs. ATP8A2 in photoreceptor cells is localized both in the perinuclear compartment of the inner segment and in the disk membranes of the outer segment (Coleman *et al*, 2009, 2014). ATP8A2 in the perinuclear compartment may produce the lipid asymmetry in the bilayer to facilitate vesicle trafficking to the disk membrane, which could explain a drastic reduction in the length of outer segments in ATP8A2-deficient mice (Coleman *et al*, 2014). Since disk membranes have a symmetrical distribution of PE and PS (Wu & Hubbell, 1993; Hessel *et al*, 2000), presumably due to significant scramblase activity of rhodopsin (Menon *et al*, 2011), ATP8A2 does not appear to play a role in generating global lipid asymmetry in disk membranes. Some portion of ATP8A2 may be transported to the disk membranes as a result of vesicle trafficking from the perinuclear compartment.

Mutations in the very low-density lipoprotein receptor (VLDLR) is also linked to CAMRQ (Ozcelik *et al*, 2008; Turkmen *et al*, 2008). VLDLR is a receptor for Reelin, an extracellular protein that guides neuronal migration in the cerebral cortex and cerebellum (Herz & Chen, 2006) and circulates between the PM and endosomes by endocytic recycling (Duit *et al*, 2010). Therefore, recycling traffic of VLDLR to the PM might be impaired in neurons without functional ATP8A2. Available antibodies failed to detect VLDLR protein in primary cortical neurons used in this study. Further studies are required to address this issue.

Materials and Methods

Antibodies

The following antibodies were purchased from the manufacturers as noted: rabbit anti-ATP8A1 and rabbit anti-ARF1 (Proteintech); mouse anti-1D4 (Millipore); mouse anti-α-tubulin, rabbit anti-GM130, and mouse anti-myc (9E10) (Sigma); mouse anti-PI(4)P (Echelon); mouse anti-GM130 and mouse anti-LAMP1 (H4A3) (BD Biosciences); mouse anti-human TfnR (H68.4; Zymed Laboratories); rabbit anti-EHD1 (epitomics); mouse anti-LAMP2 (Santa Cruz); mouse anti-CD63 (Cymbus Biotechnology); rabbit anti-myc (Upstate); goat anti-VPS26 (Everest biotech); mouse anti-6xHis (Wako); rabbit anti-syntaxin 5 (Synaptic Systems); mouse anti-TfnR antibody (13E4) (Abcam); Alexa 488-, 594-, or 647-conjugated secondary antibodies (Invitrogen); and sheep anti-mouse IgG antibody-HRP and donkey anti-rabbit IgG antibody-HRP (GE Healthcare).

Reagents

The following reagents were purchased from the manufacturers as noted: cholesterol (C8503), sulfatide, PA, ethanolamine, ATP and n-octyl-β-D-glucopyranoside (Sigma); and PI (Echelon); di16:0-PIPs (CellSignals); PS, PE, and PC (porcine brain) for liposome cosedimentation assay, 1,2-dioleoyl-PC, 1,2-dioleoyl-PE, 1,2-dioleoyl-PS, 1,2-dioleoyl-PI, 1,2-dioleoyl-PG, 1,2-dioleoyl-PA, brain polar lipids (porcine), sphingomyelin (porcine brain), cholesterol (ovine wool), C6-NBD-PS and C6-NBD-PE (Avanti Polar Lipids); dithionite (Fisher); CHAPS (Anatrace); and Alexa 594-Tfn, Alexa 594-CTxB, Alexa 555-EGF (Invitrogen). To prepare Alexa 488-Tfn, human holo-Tfn (Sigma) was conjugated with Alexa 488 using Alexa Flour succinimidyl ester (Invitrogen) and then purified by PD-10 desalting columns (GE Healthcare).

Plasmids

The following genes were amplified by polymerase chain reaction (PCR) with cDNA derived from HeLa cells using the following primers: 5′-AGCCGCCTCGAGCATGCCCACCATGCGGAGGAC-3′ (ATP8A1; sense primer, XhoI site is underlined) and 5′-AGGCTCCCCGGGTCACCATTCGTCGGGCCTC-3′ (ATP8A1; antisense primer, SmaI site is underlined); 5′-GCCTCGAGATGTTCAGCTGGGTCAGC-3′ (EHD1; sense primer, XhoI site is underlined) and 5′-GCGAATTCTCACTC ATGTCTGCGCTTG-3′ (EHD1; antisense primer, EcoRI site is underlined); 5′-TGGCAGGAATTCATGATGGATCAAGCTAGATC-3′ (TfnR; sense primer, EcoRI site is underlined) and 5′-GGTATCGGATCCC AAACTCATTGTCAATGTCCC-3′ (TfnR; antisense primer, BamHI site is underlined); 5′-GGAAGACCTGGAATTCATGGCGATGAACTA TAACG-3′ (CDC50A; sense primer, EcoRI site is underlined) and 5′-TAGATGCATGCTCGAGTTAAATGGTA ATGTCAGC-3′ (CDC50A; antisense primer, XhoI site is underlined); 5′-GCAGATCTCATGGGC ACCCGCGACGACGA-3′ (Rab11; sense primer, BglII site is underlined) and 5′-GCGTCGACTTAGATGTTC TGACAGCACT-3′ (Rab11; antisense primer). Only one isoform (NM_001105529) of ATP8A1 was amplified, which corresponds to bovine isoform β1 (Ding *et al*, 2000). The products encoding ATP8A1 and EHD1 were introduced into pEGFP-C3 and pEGFP-C2 (Clontech), respectively, to generate N-terminal GFP-tagged constructs. The product encoding TfnR was introduced into pEGFP-N2 (Clontech) to generate a C-terminal GFP-tagged construct. The product encoding CDC50A was introduced into pcDNA with myc-tag (Invitrogen) to generate an N-terminal myc-tagged construct. The product encoding Rab11 was introduced into pmCherry-C3 (generated by the replacement of the EGFP sequence in pEGFP-C3

with an mCherry sequence) to generate an N-terminal mCherry-tagged construct. For the preparation of siRNA-resistant N-terminal GFP-tagged ATP8A1 expression vector, six silent mutations were introduced by PCR in the ATP8A1 siRNA1 target sequence (see below) using 5′-GCACCTCGAATCTGAATGAG GAACT-3′(sense primer) and 5′-GCGCCATCGCCGCAGTGTCTGTGG G-3′ (antisense primer). ATP8A1 E191Q mutant was constructed by site-directed mutagenesis of siRNA-resistant wild-type ATP8A1. Human ATP8A2 (Coleman *et al*, 2009) was introduced into pEGFP-C2 using In-Fusion HD Cloning Kit (TAKARA). ATP8A2 (E210Q or I376M) and EHD1 (K324D) were constructed by site-directed mutagenesis of wild-type ATP8A2 and EHD1, respectively. GFP-EHD1 ΔEH (1-438) was generated using 5′-GCCTCGAGATGTTCAGCTGGG TCAGC-3′ (sense primer, XhoI site is underlined) and GCGAATTC TCACTC CACGTCGTCGATGC (antisense primer, EcoRI site is underlined).

Cell culture

COS-1 cells were maintained in DMEM with 10% FBS. PSA-3 and R-41 cells were cultured in Ham's F-12 medium as previously described (Lee *et al*, 2012).

Plasmid transfection

Cells were transiently transfected with plasmids using Lipofectamine 2000 (Invitrogen) according to the manufacturer's instructions.

RNA interference

siRNA duplex oligomers were designed (Nippon EGT) as follows: GCUAUGGCUCGAACAUCUA (ATP8A1 siRNA1), CUCUGACUACUC CAUAGCU (ATP8A1 siRNA2), GGUGUAUAGGUCUCUAUAA (ATP8 A1siRNA3), GUUUCCUCGCCUCUCGAAA (EHD1 siRNA1), and CC GUCACUCCAUACAGUAU (EHD1 siRNA2). A total of 20 nM siRNA was introduced to COS-1 cells using Lipofectamine RNAiMAX (Invitrogen) according to the manufacturer's instruction. After 4 h, the medium was replaced by DMEM with 10% FBS and cells were further incubated for 72 h for subsequent experiments. Cells treated only with Lipofectamine RNAiMAX are defined as control cells.

Immunocytochemistry

Immunocytochemistry was performed as described previously (Uchida *et al*, 2011). TfnR staining was performed using anti-TfnR antibody (H68.4) unless indicated otherwise. For the stain of endogenous EHD1, cells were fixed with pre-warmed 2% paraformaldehyde in PBS at room temperature for 10 min, quenched with 50 mM NH_4Cl, and permeabilized with 0.1% Triton X-100 in PBS at room temperature for 5 min. After blocking with 3% BSA in PBS, cells were incubated with rabbit anti-EHD1 antibody. For ARF1 staining, fixed and permeabilized cells were incubated with the primary antibody in Can Get Signal immunostain solution A (TOYOBO). For LAMP1 and PI4P staining, fixed cells were permeabilized with 20 μM digitonin in PBS for 5 min at room temperature before blocking. Rab11 staining was performed as previously described (Lee *et al*, 2012).

Establishment of COS-1 cells stably expressing GFP-lact-C2

GFP-lact-C2 was amplified from lact-C2 in pEGFP-C2 vector (Uchida *et al*, 2011) using 5′-GCAGACAAGCTTCGCCACCATGGTGAGCAA GG-3′ (sense primer) and 5′-GCAGACATCGATCTAACAGCCCAGCA GCTCC-3′ (antisense primer), and subsequently cloned into pLHCX (Clontech) at HindIII/ClaI. Recombinant retrovirus harboring GFP-lact-C2 was prepared using a retrovirus packaging kit ampho (Takara-bio) according to the manufacturer's instructions. In brief, pLHCX/GFP-lact-C2 was transfected into HEK293T cells in combination with pGP (encoding gag and pol) and pE-ampho (encoding amphotropic env). The conditioned medium containing recombinant retrovirus particle was collected, then filtrated with 0.4-μm membrane filter to remove cell debris, and stored at 4°C before use. COS-1 cells were infected with EGFP-lact-C2 retrovirus in DMEM with 10% FBS and 8 μg/ml polybrene, and cells were subjected to drug-selection with 200 μg/ml hygromycin for 2 weeks. The hygromycin-resistant colonies were then picked up.

Visualization of PS at the luminal leaflet

COS-1 cells that were transiently or stably expressing GFP-lact-C2 were fixed with 3.7% formaldehyde in PBS at room temperature for 15 min and permeabilized with 0.1% saponin in PBS at room temperature for 10 min. After blocking with 3% BSA in PBS, cells were treated with recombinant 2xPH-6xHis (2 μg/ml), mouse anti-6xHis tag (1:1,000), and rabbit anti-GM130 at 4°C overnight. After washing with PBS, cells were incubated with anti-mouse IgG conjugated with Alexa 594 and anti-rabbit IgG conjugated with Alexa 647 at room temperature for 1 h, washed with PBS, and then mounted. Intensity of recombinant 2xPH-6xHis in RE area was quantified with ImageJ (NIH).

Streptolysin O treatment

Cells were fixed with 2% PFA in PBS and incubated at 4°C for 15 min with 200 units/ml Streptolysin O (Sigma) in ice-cold PBS containing 10 mM DTT. Cells were then washed with ice-cold PBS containing 10 mM DTT twice, incubated in PBS containing 10 mM DTT at 37°C for 20 min., and washed with PBS.

Confocal microscopy

Confocal microscopy was performed using a LSM510 META (Carl Zeiss Microimaging) with a 63 × 1.4 Plan-Apochromat oil immersion lens, or a TCS SP8 (Leica) with a 63 × 1.2 Plan-Apochromat water immersion lens. With a TCS SP8, excitation was done with a 65 mW Argon laser emitting at 488 nm. Emissions were collected from 500 to 600 nm using Spectral detector.

Tfn recycling assay

COS-1 cells were first incubated in serum-free medium for 30 min at 37°C and subsequently in medium containing 200 μg/ml Alexa 488 or 594-Tfn for 60 min. After washing with ice-cold PBS, cells were incubated in 'acid-wash buffer' (20 mM sodium-acetate buffer, 1 mM $CaCl_2$, 150 mM NaCl, pH 4.8) on ice for 5 min to remove surface-bound transferrin. Cells were washed with ice-cold PBS and

chased in phenol red-free DMEM containing 400 μg/ml unlabeled human holo-Tfn at 37°C with 5% CO2. During the chase, cells were imaged every 3 or 6 min for 1 h with a TCS SP8. The perinuclear fluorescence intensity of Alexa 488 or 594 minus the background fluorescence intensity was quantified with ImageJ.

Live imaging for TfnR-GFP in xyt mode

COS-1 cells expressing TfnR-GFP were placed in phenol red-free DMEM/10% FBS. Cells were imaged in xyt mode at 37°C with 5% CO_2 using a TCS SP8. After the photobleach with 100% power of 488 nm laser for 10 s exposure, the images were collected every 0.5 s for 1–2 min.

Epifluorescence microscopy imaging system based on an inverted microscope (IX81-ZDC; Olympus), 150 × NA 1.45 TIRFM objective (Olympus), motorized filter wheel (Olympus), electron multiplying charge coupled device camera (iXon; Andor), 488 nm laser line and a MetaMorph software (MDS Analytical Technologies). The emission filter 531/46 nm with 488 nm laser for acquisition of EGFP-streaming images was used.

Expression and purification of ATP8A1 and ATP8A2

Expression, purification, and reconstitution of ATP8A1 (WT and E191Q) and ATP8A2 (WT and I376M) containing the nine amino acid 1D4 C-terminal tag were performed as described previously Coleman *et al* (2009).

ATPase assay

ATPase activity was measured as described Coleman *et al* (2009). In brief, immunoaffinity-purified ATP8A1 or ATP8A2 in PC with increasing amounts of PS was assayed in 50 mM HEPES-NaOH (pH 7.5), 150 mM NaCl, 12.5 mM $MgCl_2$, 1 mM DTT, 5 mM ATP, and 10 mM CHAPS at 37°C. The total lipid concentration was kept constant at 2.5 mg/ml. Assays were terminated by the addition of 6% (wt/vol) SDS. The release of phosphate from ATP was determined using the colorimetric microplate method (Gonzalez-Romo *et al*, 1992).

Flippase assay

Flippase assays were performed as described (Coleman *et al*, 2009; Coleman & Molday, 2011) with ATP8A1 or ATP8A2 reconstituted in liposome consisting of 97.5% PC and 2.5% fluorescently labeled (NBD) PS or PE.

Expression and purification of recombinant proteins

WT or mutant EHD1 cDNA was subcloned into pET-45b (Novagen), and the N-terminal His-tagged protein was expressed in *E. coli* Arctic Express (DE3) RP cells (Agilent Technologies). Bacterial cultures in LB medium were induced with 1 mM IPTG and grown overnight at 13°C. The protein was purified using a HisTrap HP column (GE Healthcare) according to the manufacturer's instructions and then dialyzed against 20 mM HEPES-NaOH (pH 7.5) containing 300 mM NaCl, 1 mM $MgCl_2$, and 1 mM DTT.

The sequence encoding a tandem fusion of evt-2 PH domain (2xPH) was introduced into pET-21a (Novagen), and the C-terminal His-tagged protein was expressed in *E. coli* BL21 (DE3) cells. Bacterial cultures in LB medium were induced with 1 mM IPTG and grown overnight at 20°C. The protein was purified using a HisTrap HP column and then dialyzed against PBS.

Liposome co-sedimentation assay

The liposome co-sedimentation assay using His-tagged 2xPH was performed as previously described (Uchida *et al*, 2011) with modifications. Lipid mixtures were dried under nitrogen gas and hydrated in 25 mM HEPES-NaOH (pH 7.5) containing 100 mM NaCl and 0.5 mM EDTA for 90 min at 37°C, and vortexed briefly. To remove protein aggregates, the protein solution was subjected to centrifugation at 100,000 *g* for 30 min at 4°C. 10 μg of proteins were incubated with 65 nmol liposomes in the buffer (50 μl) for 15 min at room temperature, and the mixture was centrifuged at 100,000 *g* for 30 min at 20°C. The resultant supernatant and pellet were subjected to SDS–PAGE, and the proteins and lipids were stained with Coomassie blue. Lipid stain was observed just below bromophenol blue. As a negative control, a sample without liposomes was subjected to the same procedure.

The assay using His-tagged EHD1 was performed as described above with the following modifications: (i) dried lipid mixtures were hydrated in 20 mM HEPES-NaOH (pH 7.5) containing 100 mM NaCl, 1 mM $MgCl_2$, and 1 mM DTT; (ii) the protein solution was subjected to centrifugation at 100,000 *g* for 15 min at 4°C to remove aggregates; (iii) 7 μg of proteins were incubated with 50 nmol liposomes.

The intensities of individual bands were quantified with ImageJ. The band intensity in the pellet fraction of the sample without liposomes (a) was subtracted from that of the sample with liposomes (Ippt) to calculate the amount of bound protein (Ippt − a). The percentage of the bound protein was obtained by the following equation: %bound = 100 × (Ippt − a) / [Isup + (Ippt − a)], where Isup represents the band intensity in the supernatant fraction. The binding data from two independent experiments were analyzed by fitting to the 'one-site specific binding with Hill slope' equation in GraphPad Prism 5 (GraphPad Software). $Y = B_{max} \times Xh / (kh + Xh)$, where k and h represent the concentration of PS resulting in half-maximal binding and the Hill coefficient, respectively.

To prepare liposomes of decreasing size, dried lipid mixtures containing 1% (mol/mol) rhodamine-labelled PE (Avanti) were hydrated in 20 mM HEPES-NaOH (pH 7.5) containing 100 mM NaCl, 1 mM $MgCl_2$, and 1 mM DTT and then dipped into liquid nitrogen for rapid cooling. After completely frozen, the lipids were transferred to a bath at 37°C for thawing. After completely thawed, the lipids were frozen again. This freeze–thaw operation was repeated three times. The lipids were then extruded through 400 nm or 100 nm polycarbonate filters (Whatman) at room temperature using Avanti mini-extruder and stored on ice for further experiments. After centrifugation with His-EHD1, the fluorescence of each supernatant was measured, and the amount of precipitated liposomes was calculated. The percentage of precipitated liposomes was used to calculate the percentage of liposome-bound His-EHD1 in Fig 5D and E. Approximately 70–95% of liposomes were precipitated.

Liposome size measurement by dynamic light scattering (DLS)

The liposome size was measured using a Zetasizer Nano ZS (Malvern) equipped with a 4 mW He–Ne laser (633 nm) and disposable cuvettes (ZEN0112, Malvern) at 25°C. The z-averaged diameter of the particles was calculated from the intensity of the scattered light using the Malvern Zetasizer software. The data of all samples met quality criteria assuming monomodal size distributions.

Western blotting

Western blotting was performed as described previously (Uchida *et al*, 2011).

CTxB retrograde traffic assay

CTxB retrograde traffic assay was performed as described previously (Uchida *et al*, 2011).

EGF traffic assay

Cells were pre-incubated in serum-free DMEM for 30 min at 37°C and then pulsed with 2 μg/ml Alexa 555-EGF in serum-free DMEM for 5 min at 37°C. After washing, cells were chased in DMEM containing 10% FBS for 60 min at 37°C, fixed, and stained for LAMP1. Pearson's coefficient between Alexa 555-EGF and LAMP1 was determined with ImageJ.

Cortical neuron culture

Cortical neurons were obtained from *Atp8a2*$^{+/+}$ or *Atp8a2*$^{-/-}$ mice (embryonic day 15–17) as previously described (Koie *et al*, 2014). In brief, 6-well plate dishes were coated with 0.01% poly-L-lysine hydrobromide (Sigma) in PBS for overnight at 37°C and subsequently washed four times with water. Cerebral cortices were trypsinized for 5 min at 37°C, treated with 2 U/μl DNase I (Invitrogen), and dissociated by triturating with fire-polished Pasteur pipette. The neurons were cultured in Neurobasal medium (Invitrogen) containing 2% B27 supplement (Invitrogen), 2 mM Glutamax (Invitrogen), and antibiotics for 4 days.

Biotinylation assay

For surface biotinylation, cortical neurons (4 DIV) were cooled on ice, washed three times with ice-cold PBS containing 1 mM $CaCl_2$ and 0.5 mM $MgCl_2$, and then incubated with PBS containing 1 mM $CaCl_2$, 0.5 mM $MgCl_2$, and 1 mg/ml EZ-link Sulfo-NHS-SS-Biotin (Thermo) for 40 min at 4°C. Unreacted biotin was quenched by washing cells with ice-cold PBS containing 100 mM glycine, and then cells were washed twice with ice-cold PBS. Cells were harvested in lysis buffer (20 mM Tris-HCl pH 7.4, 5 mM EDTA, 100 mM NaCl, 1% Triton X-100, 0.1% SDS) with complete protease inhibitor cocktail (Roche). Homogenates were centrifuged at 13,000 rpm for 10 min at 4°C. 10% of the resulting supernatant was stored as the total fraction. The remaining 85% of the supernatant was rotated for 1 h at 4°C with NeutrAvidin agarose resin (Thermo) and centrifuged at 500 *g* for 1 min at 4°C. Precipitates were washed three times with wash buffer (25 mM HEPES, 150 mM NaCl, 5 mM EDTA, 0.1% Triton X-100) and stored as the surface fraction. Both total and surface protein samples were boiled for 5 min at 95°C. Western blotting was performed and band intensities were quantified with ImageJ. The ratio of surface to total TfnR or tubulin was calculated, and that of tubulin was subtracted from that of TfnR to exclude the amount of cytoplasmic protein in the surface fraction. The calculated value was then normalized to that of *Atp8a2*$^{+/+}$.

Statistical analysis

Statistical comparisons of means were made using two-tailed Student's *t*-test or one-way ANOVA. $P < 0.05$ was used as the criterion for statistical significance.

Supplementary information for this article is available online: http://emboj.embopress.org

Acknowledgements

We thank B. Grant (Rutgers University) for anti-EHD1 antibody and critical reading of the manuscript. We also thank O. Kuge (Kyushu University), K. Emoto (University of Tokyo), and M. Umeda (Kyoto University) for kindly giving PSA-3 cells and R-41 cells; M. Hattori, T. Kohno, and K. Okumura (Nagoya city University) for critical support in primary neuron culture; A. Makino (RIKEN) for helpful support in liposome experiments; and J. McKenzie (State of California Department of Pesticide Regulation) for comments on the manuscript. We thank all members in the Molday laboratory, especially L. L. Molday for technical support and K. Chang for management of *Atp8a2*$^{-/-}$ mice. Supported by the Program for Promotion of Basic and Applied Researches for Innovations in Bio-oriented Industry (to H.A.), and Grants-in-aid from the Japanese Ministry of Education, Culture, Sports, Science, and Technology (20370045 to H.A.), Canadian Institutes of Health Research Grant (MOP-106667 to R.M.), and National Institutes of Health (EY002422 to R.M.).

Author contribution

SL, YU, JW, TKi, and KM performed experiments; TM, TN, and TKo provided reagents; SL, YU, TI, RM, TT, and HA designed research; SL, YU, TT, and HA wrote the manuscript.

Conflict of interest

The authors declare that they have no conflict of interest.

References

Balasubramanian K, Schroit AJ (2003) Aminophospholipid asymmetry: a matter of life and death. *Annu Rev Physiol* 65: 701–734

Behnia R, Munro S (2005) Organelle identity and the signposts for membrane traffic. *Nature* 438: 597–604

Bigay J, Antonny B (2012) Curvature, lipid packing, and electrostatics of membrane organelles: defining cellular territories in determining specificity. *Dev Cell* 23: 886–895

Blume JJ, Halbach A, Behrendt D, Paulsson M, Plomann M (2007) EHD proteins are associated with tubular and vesicular compartments and interact with specific phospholipids. *Exp Cell Res* 313: 219–231

Boucrot E, Pick A, Camdere G, Liska N, Evergren E, McMahon HT, Kozlov MM (2012) Membrane fission is promoted by insertion of amphipathic helices and is restricted by crescent BAR domains. *Cell* 149: 124–136

Bryde S, Hennrich H, Verhulst PM, Devaux PF, Lenoir G, Holthuis JC (2010) CDC50 proteins are critical components of the human class-1 P4-ATPase transport machinery. *J Biol Chem* 285: 40562 – 40572

Bull LN, van Eijk MJ, Pawlikowska L, DeYoung JA, Juijn JA, Liao M, Klomp LW, Lomri N, Berger R, Scharschmidt BF, Knisely AS, Houwen RH, Freimer NB (1998) A gene encoding a P-type ATPase mutated in two forms of hereditary cholestasis. *Nat Genet* 18: 219 – 224

Cacciagli P, Haddad MR, Mignon-Ravix C, El-Waly B, Moncla A, Missirian C, Chabrol B, Villard L (2010) Disruption of the ATP8A2 gene in a patient with a t(10;13) de novo balanced translocation and a severe neurological phenotype. *Eur J Hum Genet* 18: 1360 – 1363

Cai B, Caplan S, Naslavsky N (2012) cPLA2alpha and EHD1 interact and regulate the vesiculation of cholesterol-rich, GPI-anchored, protein-containing endosomes. *Mol Biol Cell* 23: 1874 – 1888

Cai B, Giridharan SS, Zhang J, Saxena S, Bahl K, Schmidt JA, Sorgen PL, Guo W, Naslavsky N, Caplan S (2013) Differential roles of C-terminal Eps15 homology domain proteins as vesiculators and tubulators of recycling endosomes. *J Biol Chem* 288: 30172 – 30180

Caplan S, Naslavsky N, Hartnell LM, Lodge R, Polishchuk RS, Donaldson JG, Bonifacino JS (2002) A tubular EHD1-containing compartment involved in the recycling of major histocompatibility complex class I molecules to the plasma membrane. *EMBO J* 21: 2557 – 2567

Chen B, Jiang Y, Zeng S, Yan J, Li X, Zhang Y, Zou W, Wang X (2010) Endocytic sorting and recycling require membrane phosphatidylserine asymmetry maintained by TAT-1/CHAT-1. *PLoS Genet* 6: e1001235

Coleman JA, Kwok MC, Molday RS (2009) Localization, purification, and functional reconstitution of the P4-ATPase Atp8a2, a phosphatidylserine flippase in photoreceptor disc membranes. *J Biol Chem* 284: 32670 – 32679

Coleman JA, Molday RS (2011) Critical role of the beta-subunit CDC50A in the stable expression, assembly, subcellular localization, and lipid transport activity of the P4-ATPase ATP8A2. *J Biol Chem* 286: 17205 – 17216

Coleman JA, Vestergaard AL, Molday RS, Vilsen B, Peter Andersen J (2012) Critical role of a transmembrane lysine in aminophospholipid transport by mammalian photoreceptor P4-ATPase ATP8A2. *Proc Natl Acad Sci USA* 109: 1449 – 1454

Coleman JA, Quazi F, Molday RS (2013) Mammalian P4-ATPases and ABC transporters and their role in phospholipid transport. *Biochim Biophys Acta* 1831: 555 – 574

Coleman JA, Zhu X, Djajadi HR, Molday LL, Smith RS, Libby RT, John SW, Molday RS (2014) Phospholipid flippase ATP8A2 is required for normal visual and auditory function and photoreceptor and spiral ganglion cell survival. *J Cell Sci* 127: 1138 – 1149

Daumke O, Lundmark R, Vallis Y, Martens S, Butler PJ, McMahon HT (2007) Architectural and mechanistic insights into an EHD ATPase involved in membrane remodelling. *Nature* 449: 923 – 927

Devaux PF (1992) Protein involvement in transmembrane lipid asymmetry. *Annu Rev Biophys Biomol Struct* 21: 417 – 439

Di Paolo G, De Camilli P (2006) Phosphoinositides in cell regulation and membrane dynamics. *Nature* 443: 651 – 657

Ding J, Wu Z, Crider BP, Ma Y, Li X, Slaughter C, Gong L, Xie XS (2000) Identification and functional expression of four isoforms of ATPase II, the putative aminophospholipid translocase. Effect of isoform variation on the ATPase activity and phospholipid specificity. *J Biol Chem* 275: 23378 – 23386

Dodge JT, Phillips GB (1967) Composition of phospholipids and of phospholipid fatty acids and aldehydes in human red cells. *J Lipid Res* 8: 667 – 675

Duit S, Mayer H, Blake SM, Schneider WJ, Nimpf J (2010) Differential functions of ApoER2 and very low density lipoprotein receptor in Reelin signaling depend on differential sorting of the receptors. *J Biol Chem* 285: 4896 – 4908

Emoto K, Umeda M (2000) An essential role for a membrane lipid in cytokinesis. Regulation of contractile ring disassembly by redistribution of phosphatidylethanolamine. *J Cell Biol* 149: 1215 – 1224

Fairn GD, Schieber NL, Ariotti N, Murphy S, Kuerschner L, Webb RI, Grinstein S, Parton RG (2011) High-resolution mapping reveals topologically distinct cellular pools of phosphatidylserine. *J Cell Biol* 194: 257 – 275

Gagescu R, Demaurex N, Parton RG, Hunziker W, Huber LA, Gruenberg J (2000) The recycling endosome of Madin-Darby canine kidney cells is a mildly acidic compartment rich in raft components. *Mol Biol Cell* 11: 2775 – 2791

Gelabert-Baldrich M, Soriano-Castell D, Calvo M, Lu A, Vina-Vilaseca A, Rentero C, Pol A, Grinstein S, Enrich C, Tebar F (2014) Dynamics of KRas on endosomes: involvement of acidic phospholipids in its association. *FASEB J* 28: 3023 – 3037

Giridharan SS, Cai B, Vitale N, Naslavsky N, Caplan S (2013) Cooperation of MICAL-L1, syndapin2, and phosphatidic acid in tubular recycling endosome biogenesis. *Mol Biol Cell* 24: 1776 – 1790, S1

Gonzalez-Romo P, Sanchez-Nieto S, Gavilanes-Ruiz M (1992) A modified colorimetric method for the determination of orthophosphate in the presence of high ATP concentrations. *Anal Biochem* 200: 235 – 238

Graham TR (2004) Flippases and vesicle-mediated protein transport. *Trends Cell Biol* 14: 670 – 677

Grant B, Zhang Y, Paupard MC, Lin SX, Hall DH, Hirsh D (2001) Evidence that RME-1, a conserved C. elegans EH-domain protein, functions in endocytic recycling. *Nat Cell Biol* 3: 573 – 579

Grant BD, Caplan S (2008) Mechanisms of EHD/RME-1 protein function in endocytic transport. *Traffic* 9: 2043 – 2052

Grant BD, Donaldson JG (2009) Pathways and mechanisms of endocytic recycling. *Nat Rev Mol Cell Biol* 10: 597 – 608

Hancock JF (2003) Ras proteins: different signals from different locations. *Nat Rev Mol Cell Biol* 4: 373 – 384

Herz J, Chen Y (2006) Reelin, lipoprotein receptors and synaptic plasticity. *Nat Rev Neurosci* 7: 850 – 859

Hessel E, Herrmann A, Muller P, Schnetkamp PP, Hofmann KP (2000) The transbilayer distribution of phospholipids in disc membranes is a dynamic equilibrium evidence for rapid flip and flop movement. *Eur J Biochem* 267: 1473 – 1483

Holthuis JC, Levine TP (2005) Lipid traffic: floppy drives and a superhighway. *Nat Rev Mol Cell Biol* 6: 209 – 220

Holthuis JC, Menon AK (2014) Lipid landscapes and pipelines in membrane homeostasis. *Nature* 510: 48 – 57

Huang BX, Akbar M, Kevala K, Kim HY (2011) Phosphatidylserine is a critical modulator for Akt activation. *J Cell Biol* 192: 979 – 992

Kato U, Inadome H, Yamamoto M, Emoto K, Kobayashi T, Umeda M (2013) Role for phospholipid flippase complex of ATP8A1 and CDC50A proteins in cell migration. *J Biol Chem* 288: 4922 – 4934

Knaevelsrud H, Soreng K, Raiborg C, Haberg K, Rasmuson F, Brech A, Liestol K, Rusten TE, Stenmark H, Neufeld TP, Carlsson SR, Simonsen A (2013) Membrane remodeling by the PX-BAR protein SNX18 promotes autophagosome formation. *J Cell Biol* 202: 331 – 349

Koie M, Okumura K, Hisanaga A, Kamei T, Sasaki K, Deng M, Baba A, Kohno T, Hattori M (2014) Cleavage within Reelin repeat 3 regulates the duration and range of the signaling activity of Reelin protein. *J Biol Chem* 289: 12922 – 12930

Kuge O, Nishijima M, Akamatsu Y (1986) Phosphatidylserine biosynthesis in cultured Chinese hamster ovary cells. II. Isolation and characterization of phosphatidylserine auxotrophs. *J Biol Chem* 261: 5790 – 5794

Kuge O, Nishijima M (1997) Phosphatidylserine synthase I and II of mammalian cells. *Biochim Biophys Acta* 1348: 151 – 156

Lee S, Uchida Y, Emoto K, Umeda M, Kuge O, Taguchi T, Arai H (2012) Impaired retrograde membrane traffic through endosomes in a mutant CHO cell defective in phosphatidylserine synthesis. *Genes Cells* 17: 728 – 736

Lin SX, Grant B, Hirsh D, Maxfield FR (2001) Rme-1 regulates the distribution and function of the endocytic recycling compartment in mammalian cells. *Nat Cell Biol* 3: 567 – 572

Longatti A, Lamb CA, Razi M, Yoshimura S, Barr FA, Tooze SA (2012) TBC1D14 regulates autophagosome formation via Rab11- and ULK1-positive recycling endosomes. *J Cell Biol* 197: 659 – 675

Lu A, Tebar F, Alvarez-Moya B, Lopez-Alcala C, Calvo M, Enrich C, Agell N, Nakamura T, Matsuda M, Bachs O (2009) A clathrin-dependent pathway leads to KRas signaling on late endosomes en route to lysosomes. *J Cell Biol* 184: 863 – 879

Maeda K, Anand K, Chiapparino A, Kumar A, Poletto M, Kaksonen M, Gavin AC (2013) Interactome map uncovers phosphatidylserine transport by oxysterol-binding proteins. *Nature* 501: 257 – 261

Maxfield FR, McGraw TE (2004) Endocytic recycling. *Nat Rev Mol Cell Biol* 5: 121 – 132

McKenzie JE, Raisley B, Zhou X, Naslavsky N, Taguchi T, Caplan S, Sheff D (2012) Retromer Guides STxB and CD8-M6PR from Early to Recycling Endosomes, EHD1 Guides STxB from Recycling Endosome to Golgi. *Traffic* 13: 1140 – 1159

Mellman I (1996) Endocytosis and molecular sorting. *Annu Rev Cell Dev Biol* 12: 575 – 625

Menon I, Huber T, Sanyal S, Banerjee S, Barre P, Canis S, Warren JD, Hwa J, Sakmar TP, Menon AK (2011) Opsin is a phospholipid flippase. *Curr Biol* 21: 149 – 153

Misaki R, Nakagawa T, Fukuda M, Taniguchi N, Taguchi T (2007) Spatial segregation of degradation- and recycling-trafficking pathways in COS-1 cells. *Biochem Biophys Res Commun* 360: 580 – 585

Mondal M, Mesmin B, Mukherjee S, Maxfield FR (2009) Sterols are mainly in the cytoplasmic leaflet of the plasma membrane and the endocytic recycling compartment in CHO cells. *Mol Biol Cell* 20: 581 – 588

Natarajan P, Liu K, Patil DV, Sciorra VA, Jackson CL, Graham TR (2009) Regulation of a Golgi flippase by phosphoinositides and an ArfGEF. *Nat Cell Biol* 11: 1421 – 1426

Newton AC, Keranen LM (1994) Phosphatidyl-L-serine is necessary for protein kinase C's high-affinity interaction with diacylglycerol-containing membranes. *Biochemistry* 33: 6651 – 6658

Onat OE, Gulsuner S, Bilguvar K, Nazli Basak A, Topaloglu H, Tan M, Tan U, Gunel M, Ozcelik T (2013) Missense mutation in the ATPase, aminophospholipid transporter protein ATP8A2 is associated with cerebellar atrophy and quadrupedal locomotion. *Eur J Hum Genet* 21: 281 – 285

Ozcelik T, Akarsu N, Uz E, Caglayan S, Gulsuner S, Onat OE, Tan M, Tan U (2008) Mutations in the very low-density lipoprotein receptor VLDLR cause cerebellar hypoplasia and quadrupedal locomotion in humans. *Proc Natl Acad Sci USA* 105: 4232 – 4236

Pant S, Sharma M, Patel K, Caplan S, Carr CM, Grant BD (2009) AMPH-1/Amphiphysin/Bin1 functions with RME-1/Ehd1 in endocytic recycling. *Nat Cell Biol* 11: 1399 – 1410

Paterson JK, Renkema K, Burden L, Halleck MS, Schlegel RA, Williamson P, Daleke DL (2006) Lipid specific activation of the murine P4-ATPase Atp8a1 (ATPase II). *Biochemistry* 45: 5367 – 5376

Pomorski T, Lombardi R, Riezman H, Devaux PF, van Meer G, Holthuis JC (2003) Drs2p-related P-type ATPases Dnf1p and Dnf2p are required for phospholipid translocation across the yeast plasma membrane and serve a role in endocytosis. *Mol Biol Cell* 14: 1240 – 1254

Poulsen LR, Lopez-Marques RL, McDowell SC, Okkeri J, Licht D, Schulz A, Pomorski T, Harper JF, Palmgren MG (2008) The Arabidopsis P4-ATPase ALA3 localizes to the golgi and requires a beta-subunit to function in lipid translocation and secretory vesicle formation. *Plant Cell* 20: 658 – 676

Puri C, Renna M, Bento CF, Moreau K, Rubinsztein DC (2013) Diverse autophagosome membrane sources coalesce in recycling endosomes. *Cell* 154: 1285 – 1299

Ruaud AF, Nilsson L, Richard F, Larsen MK, Bessereau JL, Tuck S (2009) The C. elegans P4-ATPase TAT-1 regulates lysosome biogenesis and endocytosis. *Traffic* 10: 88 – 100

Schmick M, Vartak N, Papke B, Kovacevic M, Truxius DC, Rossmannek L, Bastiaens PI (2014) KRas localizes to the plasma membrane by spatial cycles of solubilization, trapping and vesicular transport. *Cell* 157: 459 – 471

Sebastian TT, Baldridge RD, Xu P, Graham TR (2012) Phospholipid flippases: building asymmetric membranes and transport vesicles. *Biochim Biophys Acta* 1821: 1068 – 1077

Sharma M, Giridharan SS, Rahajeng J, Naslavsky N, Caplan S (2009) MICAL-L1 links EHD1 to tubular recycling endosomes and regulates receptor recycling. *Mol Biol Cell* 20: 5181 – 5194

Siggs OM, Arnold CN, Huber C, Pirie E, Xia Y, Lin P, Nemazee D, Beutler B (2011) The P4-type ATPase ATP11C is essential for B lymphopoiesis in adult bone marrow. *Nat Immunol* 12: 434 – 440

Soupene E, Kemaladewi DU, Kuypers FA (2008) ATP8A1 activity and phosphatidylserine transbilayer movement. *J Receptor Ligand Channel Res* 1: 1 – 10

Taguchi T (2013) Emerging roles of recycling endosomes. *J Biochem* 153: 505 – 510

Takatsu H, Baba K, Shima T, Umino H, Kato U, Umeda M, Nakayama K, Shin HW (2011) ATP9B, a P4-ATPase (a putative aminophospholipid translocase), localizes to the trans-Golgi network in a CDC50 protein-independent manner. *J Biol Chem* 286: 38159 – 38167

Tang X, Halleck MS, Schlegel RA, Williamson P (1996) A subfamily of P-type ATPases with aminophospholipid transporting activity. *Science* 272: 1495 – 1497

Turkmen S, Hoffmann K, Demirhan O, Aruoba D, Humphrey N, Mundlos S (2008) Cerebellar hypoplasia, with quadrupedal locomotion, caused by mutations in the very low-density lipoprotein receptor gene. *Eur J Hum Genet* 16: 1070 – 1074

Uchida Y, Hasegawa J, Chinnapen D, Inoue T, Okazaki S, Kato R, Wakatsuki S, Misaki R, Koike M, Uchiyama Y, Iemura S, Natsume T, Kuwahara R, Nakagawa T, Nishikawa K, Mukai K, Miyoshi E, Taniguchi N, Sheff D, Lencer WI *et al* (2011) Intracellular phosphatidylserine is essential for retrograde membrane traffic through endosomes. *Proc Natl Acad Sci USA* 108: 15846 – 15851

Vance JE, Steenbergen R (2005) Metabolism and functions of phosphatidylserine. *Prog Lipid Res* 44: 207 – 234

van der Velden LM, Wichers CG, van Breevoort AE, Coleman JA, Molday RS, Berger R, Klomp LW, van de Graaf SF (2010) Heteromeric interactions required for abundance and subcellular localization of human CDC50 proteins and class 1 P4-ATPases. *J Biol Chem* 285: 40088 – 40096

Vestergaard AL, Coleman JA, Lemmin T, Mikkelsen SA, Molday LL, Vilsen B, Molday RS, Dal Peraro M, Andersen JP (2014) Critical roles of isoleucine-364 and adjacent residues in a hydrophobic gate control of phospholipid transport by the mammalian P4-ATPase ATP8A2. *Proc Natl Acad Sci USA* 111: E1334 – E1343

Wu G, Hubbell WL (1993) Phospholipid asymmetry and transmembrane diffusion in photoreceptor disc membranes. *Biochemistry* 32: 879 – 888

Xu P, Baldridge RD, Chi RJ, Burd CG, Graham TR (2013) Phosphatidylserine flipping enhances membrane curvature and negative charge required for vesicular transport. *J Cell Biol* 202: 875 – 886

Yabas M, Teh CE, Frankenreiter S, Lal D, Roots CM, Whittle B, Andrews DT, Zhang Y, Teoh NC, Sprent J, Tze LE, Kucharska EM, Kofler J, Farell GC, Broer S, Goodnow CC, Enders A (2011) ATP11C is critical for the internalization of phosphatidylserine and differentiation of B lymphocytes. *Nat Immunol* 12: 441 – 449

Yamashiro DJ, Tycko B, Fluss SR, Maxfield FR (1984) Segregation of transferrin to a mildly acidic (pH 6.5) para-Golgi compartment in the recycling pathway. *Cell* 37: 789 – 800

Yeung T, Gilbert GE, Shi J, Silvius J, Kapus A, Grinstein S (2008) Membrane phosphatidylserine regulates surface charge and protein localization. *Science* 319: 210 – 213

Zachowski A, Henry JP, Devaux PF (1989) Control of transmembrane lipid asymmetry in chromaffin granules by an ATP-dependent protein. *Nature* 340: 75 – 76

Zhou X, Graham TR (2009) Reconstitution of phospholipid translocase activity with purified Drs2p, a type-IV P-type ATPase from budding yeast. *Proc Natl Acad Sci USA* 106: 16586 – 16591

Zhu X, Libby RT, de Vries WN, Smith RS, Wright DL, Bronson RT, Seburn KL, John SW (2012) Mutations in a p-type ATPase gene cause axonal degeneration. *PLoS Genet* 8: e1002853